Mechanistic and evolutionary insights into isoform-specific 'supercharging' in DCLK family kinases

Aarya Venkat[1+], Grace Watterson[1+], Dominic P. Byrne[2+], Brady O'Boyle[1], Safal Shrestha[3], Nathan Gravel[3], Emma E. Fairweather[2], Leonard A. Daly[2,4], Claire Bunn[1], Wayland Yeung[3], Ishan Aggarwal[1], Samiksha Katiyar[1], Claire E. Eyers[2,4], Patrick A. Eyers[2*], and Natarajan Kannan[1,3*]

Affiliations:

[1]Department of Biochemistry and Molecular Biology, University of Georgia, Athens, GA 30602, USA
[2]Department of Biochemistry and Systems Biology, Institute of Systems, Molecular and Integrative Biology, University of Liverpool, Liverpool, L69 7ZB, UK
[3]Institute of Bioinformatics, University of Georgia, Athens, GA 30602, USA
[4]Centre for Proteome Research, Department of Biochemistry and Systems Biology, Institute of Systems, Molecular and Integrative Biology, University of Liverpool, Liverpool, L69 7ZB, UK

+ equal contributions

*Correspondence to: Natarajan Kannan, Email: nkannan@uga.edu or Patrick Eyers, Email: patrick.eyers@liverpool.ac.uk

Abstract

Catalytic signaling outputs of protein kinases are dynamically regulated by an array of structural mechanisms, including allosteric interactions mediated by intrinsically disordered segments flanking the conserved catalytic domain. The Doublecortin Like Kinases (DCLKs) are a family of microtubule-associated proteins characterized by a flexible C-terminal autoregulatory 'tail' segment that varies in length across the various human DCLK isoforms. However, the mechanism whereby these isoform-specific variations contribute to unique modes of autoregulation is not well understood. Here, we employ a combination of statistical sequence analysis, molecular dynamics simulations and *in vitro* mutational analysis to define hallmarks of DCLK family evolutionary divergence, including analysis of splice variants within the DCLK1 sub-family, which arise through alternative codon usage and serve to 'supercharge' the inhibitory potential of the DCLK1 C-tail. We identify co-conserved motifs that readily distinguish DCLKs from all other Calcium Calmodulin Kinases (CAMKs), and a 'Swiss-army' assembly of distinct motifs that tether the C-terminal tail to conserved ATP and substrate-binding regions of the catalytic domain to generate a scaffold for auto-regulation through C-tail dynamics. Consistently, deletions and mutations that alter C-terminal tail length or interfere with co-conserved interactions within the catalytic domain alter intrinsic protein stability, nucleotide/inhibitor-binding, and catalytic activity, suggesting isoform-specific regulation of activity through alternative splicing. Our studies provide a detailed framework for investigating kinome–wide regulation of catalytic output through cis-regulatory events mediated by intrinsically disordered segments, opening new avenues for the design of mechanistically-divergent DCLK1 modulators, stabilizers or degraders.

Introduction

Protein kinases are one of the largest druggable protein families comprising 1.7% of the human genome and play essential roles in regulating diverse eukaryotic cell signaling pathways (1). The Doublecortin-like kinases (DCLKs) are understudied members of the calcium/calmodulin-dependent kinase (CAMK) clade of serine-threonine kinases (2–4). There are three distinct paralogs of DCLK (1, 2, and 3), the last of which is annotated as a “dark” kinase due to the lack of information pertaining to its function (5). Human DCLK1 (also known as DCAMKL1) was initially identified in 1999 (6), followed by the cloning of human DCLK2 and 3 paralogs (7). Full-length DCLK proteins contain N-terminal Doublecortin-like (DCX) domains, microtubule-binding elements that play a role in microtubule dynamics, neurogenesis, and neuronal migration (8,9). DCLKs have garnered much interest as disease biomarkers, since they are upregulated in a variety of cancer pathologies (10–12), as well as neurodegenerative disorders such as Huntington’s Disease (13). However, the mechanisms by which DCLK activity is auto-regulated, and how and why they have diverged from other protein kinases is not well understood.

Like all protein kinases, the catalytic domain of DCLKs adopts a bi-lobal fold (4), with an N-terminal ATP binding lobe and C-terminal substrate binding region. Canonical elements within the two lobes include the DFG motif, a Lys-Glu salt bridge that is associated with the active conformation, Gly-rich loop, and ATP-binding pocket, which are all critical elements for catalysis. Many protein kinases, including CAMKs, Tyrosine Kinases (TKs) and AGCs, elaborate on these core elements with unique N-terminal and C-terminal extensions that flank these catalytic lobes (14–18), allowing them to function as allosteric regulators of catalytic activity (4). Indeed, CAMKs are archetypal examples of kinases that can exist in an active-like structural conformation, yet still remain catalytically inactive (4). This is in large part due to the presence of unique C-terminal tails that are capable of blocking ATP or substrate binding in well-studied kinases such as CAMK1 and CAMKII. In canonical CAMKs, autoinhibition may be released upon Ca/Calmodulin interaction with the CAMK C-tail, which makes the substrate-binding pocket and enzyme active-site accessible (19). In CAMKII, the N and C-terminal segments flanking the kinase domain are variable in length across different isoforms and the level of kinase autoinhibition or autoactivation has been reported to be dependent on the linker length (20). The CAMKII C-tail can be organized into an autoregulatory domain and an intrinsically disordered association domain. The autoregulatory domain

also serves as a pseudosubstrate, which physically blocks the substrate binding pocket until it is competed away by Calmodulin (21). Notably, this autoregulatory pseudosubstrate can be phosphorylated (19), and phosphorylation of the C-tail makes CAMKII insensitive to calmodulin binding. Across the CAMK group, several other kinases share autoinhibitory activity via interactions between Calcium/calmodulin binding domains and the C-terminal tail (22,23), and a major feature of these kinases is variation in the tail length across the distinct genetic isoforms.

Table 1:

Name (This Study)	Isoform number	UniProt ID	Alternate names
DCLK1.1	1	O15075-2	DCAMKL1 alpha
DCLK1.2	2	O15075-1	DCAMKL1 beta
ΔDCLK1.1	3	O15075-3	
ΔDCLK1.2	4	O15075-4	

Table 1: Names of DCLK isoforms discussed in this paper, along with their respective isoform number, UniProt identification, and alternate names that have been used.

The human genome encodes four distinct DCLK1 isoforms, termed DCLK1.1-1.4 in UniProt (**Table 1, Figure 1**, (24)), which display differential activity- and tissue-specific expression profiles. Human DCLK1.1 (also known as DCLK1 alpha) is expressed in a variety of tissues, but is enriched in cells derived from the fetal and adult brain, whereas DCLK1.2 (also known as DCLK1 beta) is expressed exclusively in the embryonic brain (25). DCLK1.3 and 1.4, which lack tandem microtubule-binding DCX domains (**Figure 1**) but are otherwise identical to DCLK1.1 and DCLK1.2, respectively, are also highly expressed in the brain. To aid with clarity, the names of the human DCLK1 genes and their isoforms used in this paper are summarized in **Table 1**. Recent structural and cellular analyses have begun to clarify the mechanisms by which the DCLK1.2 isoform is regulated by the C-tail (2, 26-27). Mechanistically, autophosphorylation of Thr 688, which is present only in the C-tail of DCLK1.2 (and DCLK1.4), blunts kinase activity and subsequently inhibits phosphorylation of the N-terminal DCX domain and thus drives DCLK microtubule association in cells. Consistently, deletion of the C-tail or mutation of Thr 688 restores DCLK1.2 kinase activity, subsequently leading to DCX domain phosphorylation and the abolition of microtubule binding. The length and sequence of the C-tail varies across the DCLK1 isoforms; however,

how these variations contribute to isoform-specific functions and how they emerged during the course of evolution is not known.

In this paper, we employ an evolutionary systems approach that combines statistical sequence analysis with experimental studies to generate new models of DCLK evolutionary divergence and functional specialization. We identify the C-terminal tail as the hallmark of DCLK functional specialization across the kingdoms of life and propose a refined model in which this regulated tail functions as a highly adaptable 'Swiss-Army knife' that can 'supercharge' multiple aspects of DCLK signaling output. Notably, a conserved segment of the C-tail functions as an isoform-specific autoinhibitory motif, which mimics ATP functions through direct tail docking to the nucleotide-binding pocket, where it forms an ordered set of interactions that aligns the catalytic (C) spine of the kinase in the absence of ATP binding. Furthermore, modelling demonstrates a phosphorylated threonine in the C-tail of DCLK1.2, which is absent in DCLK1.1, that is poised to mimic the gamma phosphate of ATP. Other segments of the tail function as a pseudosubstrate by occluding the substrate-binding pocket and tethering to key functional regions of the catalytic domain. Thermostability analysis of purified DCLK1 proteins, combined with molecular dynamics simulations, confirms major differences in thermal and dynamic profiles of the DCLK1 isoforms, while catalytic activity assays reveal how specific variations in the G-loop and C-tail can rescue DCLK1.2 from the autoinhibited conformation. Together, these studies demonstrate that isoform-specific variations in the C-terminal tail co-evolved with residues in the DCLK kinase domain, contributing to regulatory diversification and functional specialization.

Figure 1:

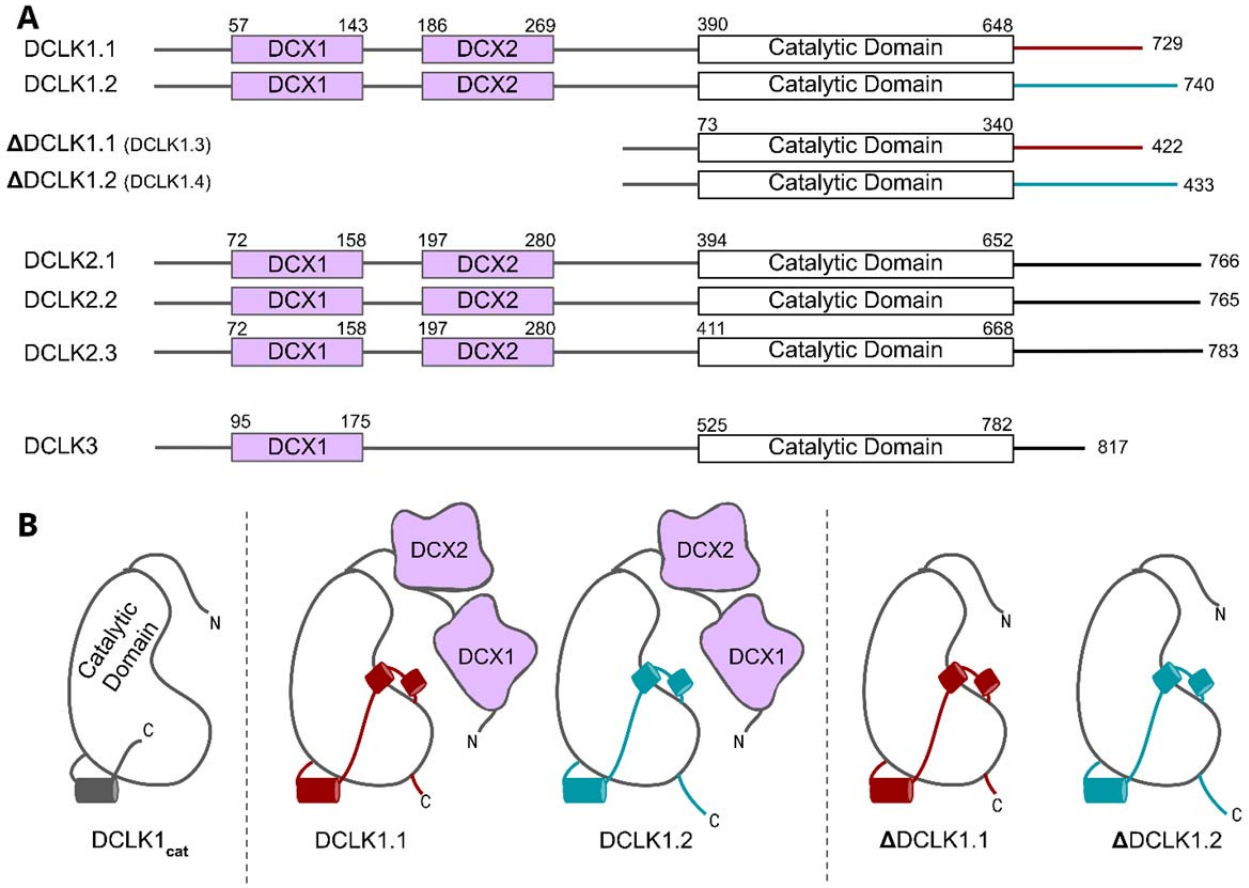

Figure 1: A) Schematic representation of domain organization for the known isoforms of the three human DCLK paralogs. Domain boundaries are annotated according to the representative amino acid sequences derived from UniProt. **B)** DCLK1 isoforms visualized as cartoons, showing key structural differences between the four human DCLK1 isoforms and a DCLK1 catalytic domain with artificially short linker regions ($DCLK1_{cat}$).

Results

Origin and evolutionary divergence of DCLK family members.

Figure 2:

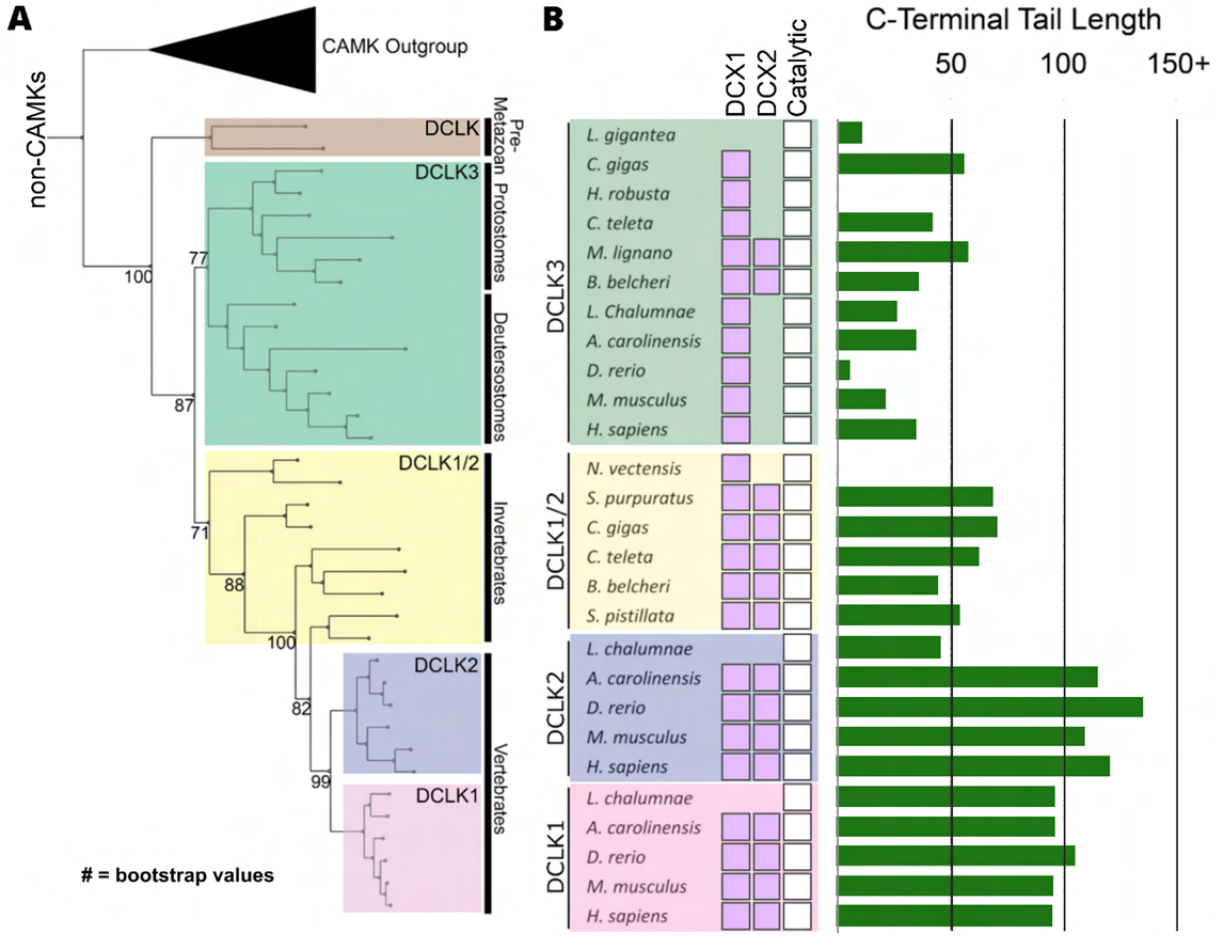

Figure 2: **Evolution of the DCLK family. A)** Phylogenetic tree showing the divergence and grouping of DCLK sub-families in different taxonomic groups. Bootstrap values are provided for each clade. **B)** Shows domain annotations for sequences included in the phylogenetic tree. The length of C-terminal tail segment for these sequences is shown as a histogram (green). The original tree generated using IQTREE is provided in **Figure 2-source data 1**.

The human DCLKs repertoire is composed of three genes, termed DCLK1, 2 and 3 (**Figure 1A**, **Table 1**). The experimental model employed in this study, DCLK1, is composed of multiple spliced variants in human cells. Those full-length proteins that contain N-terminal DCX domains are usually referred to as DCLK1.1 or DCLK1.2 and the variants that lack the DCX domains are termed here (for simplicity) ΔDCLK 1.1 and ΔDCLK1.2 (also referred to as DCLK1.3 and DCLK1.4). The core catalytic domain with minimal flanking regions ($DCLK1_{cat}$, **Figure 1B**) is identical in all DCLK1 proteins, whereas the length of the tail, or

126 the presence of the DCX domains, generates considerable diversity from the single human DCLK1 gene
127 (**Figure 1B, Figure 1-figure supplement 1**). To infer evolutionary relationships of DCLK paralogs, and
128 especially the evolution of the C-terminal tail regions that lie adjacent to the kinase domain (**Figure 1**), we
129 performed phylogenetic analysis of 36 DCLK sequences with an outgroup of closely related CAMK
130 sequences (**Figure 2A, Figure 2-source data 1**). These DCLK sequences are from a representative
131 group of holozoans, which consist of multicellular eukaryotes (metazoans) and closely related unicellular
132 eukaryotes (pre-metazoans). The analysis generated four distinct clades: pre-metazoan DCLK, metazoan
133 DCLK3, vertebrate DCLK2 and vertebrate DCLK1. Interestingly, DCLK genes demonstrated significant
134 expansion and diversification within metazoan taxa. The pre-metazoan DCLK sequences were the most
135 ancestral and showed no DCLK diversity, suggesting the DCLK expansion and diversification correlated
136 with the evolution of multicellular organisms. Within the metazoan expansion of DCLK, DCLK3 is the most
137 ancestral and can be broken down into two sub-clades: protostome DCLK3 and deuterostome DCLK3.
138 Within invertebrates, only two DCLK paralogs were present, one that was identified as a DCLK3 ortholog
139 and another that was not clearly defined as either DCLK1 or DCLK2. This suggests that the diversification
140 into DCLK1 and DCLK2 paralogs from an ancestral DCLK1/2-like paralog occurred after the divergence
141 of invertebrates and vertebrates, which his further supported by the monophyletic DCLK1 and DCLK2
142 clades in vertebrates (bootstrap value: 99).
143 Interestingly, the expansion of DCLK in metazoans and the diversification of DCLK1 and DCLK2 within
144 vertebrates correlates well with the length and sequence similarity of the C-terminal tail, which also varies
145 between the different DCLK1 splice variants (**Figure 1A, Figure 1-figure supplement 1 and 2**). Within
146 both protostome and deuterostome DCLK3, the length of the C-terminal tail is ~50 residues or less. This
147 is in marked contrast to the tail lengths of vertebrate DCLK1 and DCLK2, which are ~100 residues long.
148 In addition to the C-terminal tail, an analysis of the domain organization of these DCLKs reveals that
149 DCLK3 predominantly contains only a single N-terminal Doublecortin domain (DCX), whereas
150 invertebrate DCLKs, and vertebrate DCLK1 and DCLK2 predominantly contain two DCX domains at the
151 N-terminus of the long isoforms (**Figure 2B**). In addition, we identified a putative active site-binding motif,
152 VSVI, and a phosphorylatable threonine conserved within vertebrate DCLK1 and DCLK2, which is absent

153 in all other DCLK sequences, including invertebrate DCLK1/2. This raises the possibility that the DCLK1/2
154 tail extensions are employed for vertebrate-specific regulatory functions.
155 Next, we compared the type of DCLK1 protein sequence encoded by a range of chordate mammalian
156 genomes. The domain organization of each DCLK1 isoform was compared based on annotated
157 sequences from UniProt, demonstrating the presence of at least one DCLK1 protein that lacks the DCX
158 domains in every species examined, with a mixture of ΔDCLK1.1 and ΔDCLK1.2 splice variants.
159 Interestingly, it was only in the human DCLK1 gene that definitive evidence for ΔDCLK1.1 and ΔDCLK1.2
160 variants was found (**Figure 3A**). To establish a model for DCLK1 biophysical analysis, we constructed a
161 recombinant hybrid human DCLK1 catalytic domain with a short C-tail sequence that is equivalent to
162 DCLK1.1 amino acids 351-689, containing the catalytic domain with a short C-tail region. As shown in
163 **Figure 3B**, incubation of size-exclusion chromatography purified GST-tagged DCLK1 with 3C protease
164 generated the mature untagged DCLK1 protein for biophysical analysis. We demonstrated catalytic
165 activity for DCLK1.1$_{351-689}$ using a validated peptide phosphorylation assay (**Figure 3C**), which revealed
166 efficient phosphorylation of a DCLK1 substrate peptide. The Km [ATP] for peptide phosphorylation was
167 close to 20 μM in the presence of Mg^{2+} ions (**Figure 3C**, left panel), similar to values measured for other
168 Ser/Thr kinases that are autophosphorylated and active after expression from bacteria (28). DCLK-
169 dependent peptide phosphorylation was completely blocked (**Figure 3C**, right panel) by prior incubation
170 of the reaction mixture (containing 1mM ATP) with the chemical inhibitor DCLK1-IN-1, as expected (22).
171 In addition to enzyme activity, we monitored thermal denaturation of purified, folded, DCLK1$_{351-689}$ protein
172 in the presence of ATP, either alone or as a Mg:ATP complex, which is required for catalysis. As shown in
173 **Figure 3D**, DCLK1 was modestly stabilized by 2.1°C upon incubation with an excess of Mg:ATP, and this
174 protective effect was completely blocked by mutation of Asp 533 to Ala, consistent with canonical ATP
175 interaction in the nucleotide-binding site. Finally, we assessed the thermal effects of a panel of DCLK1
176 inhibitors on the model DCLK1.1$_{351-689}$ protein. Prior incubation with DCLK1-IN-1, LRRK2-IN-1, the
177 benzopyrimidodiazipinones XMD8-92 and XMD8-85, all of which have been reported to potently (though
178 not specifically) inhibit DCLK1 activity (27), led to marked protection from thermal unfolding (**Figure 3-
179 figure supplement 1**). Consistently, the negative control compound DCLK1-Neg (29) was ineffective in
180 stabilizing DCLK1.

Figure 3:

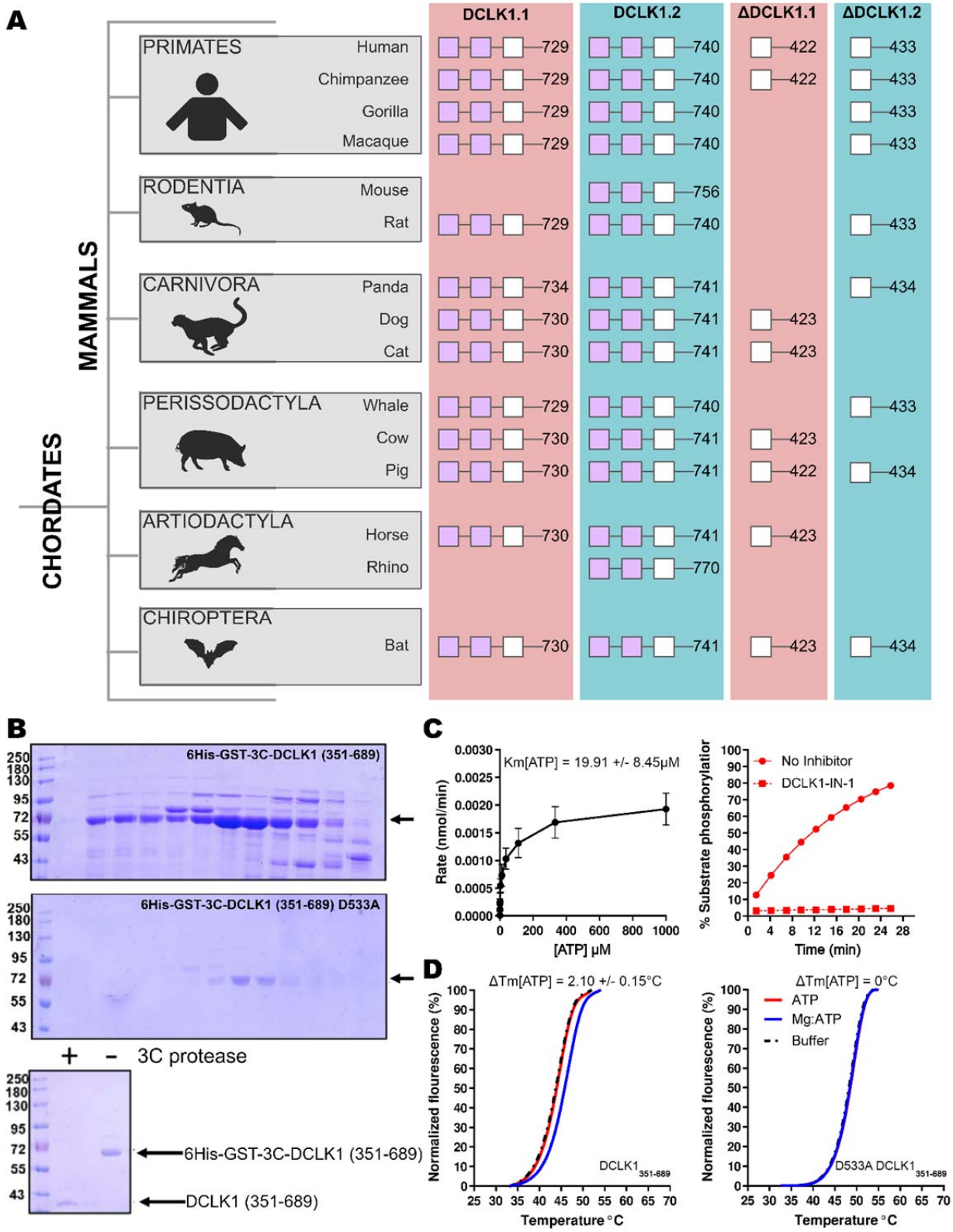
A
DCLK1.1
DCLK1.2
ΔDCLK1.1
ΔDCLK1.2
CHORDATES
MAMMALS
PRIMATES
Human
Chimpanzee
Gorilla
Macaque
RODENTIA
Mouse
Rat
CARNIVORA
Panda
Dog
Cat
PERISSODACTYLA
Whale
Cow
Pig
ARTIODACTYLA
Horse
Rhino
CHIROPTERA
Bat
B
6His-GST-3C-DCLK1 (351-689)
6His-GST-3C-DCLK1 (351-689) D533A
+ - 3C protease
6His-GST-3C-DCLK1 (351-689)
DCLK1 (351-689)
C
Km[ATP] = 19.91 +/- 8.45μM
Rate (nmol/min)
[ATP] μM
No Inhibitor
DCLK1-IN-1
% Substrate phosphorylation
Time (min)
D
ΔTm[ATP] = 2.10 +/- 0.15°C
Normalized flourescence (%)
Temperature °C
ΔTm[ATP] = 0°C
ATP
Mg:ATP
Buffer
D533A DCLK1351-689

Figure 3: **A)** Cartoon cladogram of mammalian species showing the domain organization of each DCLK1 isoform from representative annotated sequences from UniProt. UniProt IDs for each sequence are provided in **Figure 3-Source File 1**. **B)** SDS-PAGE of 6His-GST-3C-DCLK1.1 (351-689, Top) or a D533A mutant in which the DFG Asp is mutated to Ala (Middle). Proteins were separated by size exclusion chromatography, and high-purity fractions were pooled. The affinity tag was removed prior to analysis by incubation with 3C protease, leading to a demonstrable shift in mobility (bottom) **C)** Evaluation of catalytic activity towards DCLK1 peptide. DCLK1.1 351-689 possesses a Km [ATP] ~20 μM in vitro (left) and real-time substrate phosphorylation was inhibited by prior incubation with the small molecule DCLK1-IN-1, right). **D)** Thermal shift assay demonstrating a 2.1°C increase in the stability of DCLK1 351-689 in the presence of Mg:ATP (left), which was absent in the D533A protein (right). Raw data are provided in **Figure 3-Source File 2**.

Key differences between isoforms in the C-tail of DCLK1 arise from alternative-splicing and different open-reading frames

Figure 4:

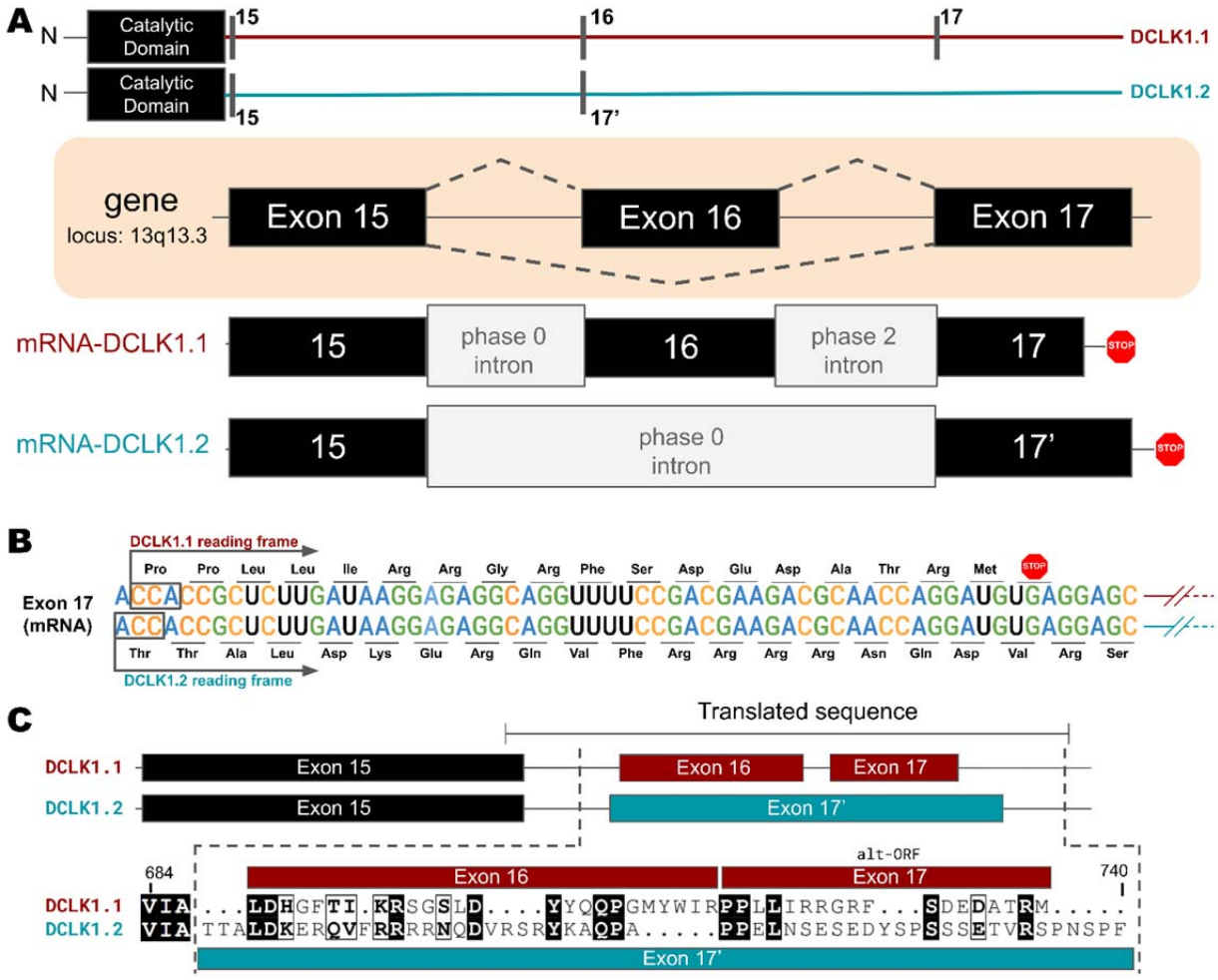

Figure 4: **A)** Gene and intron-exon organization of DCLK1 human isoforms in the C-terminal tail. The DCLK1 gene is present on locus 13q13.3, and isoforms 1 and 3, contain an additional exon (exon 16), in the C-terminal tail that is absent in DCLK1.2. **B)** A phase 2 intron results in the alternative transcript of exon 17 in isoform 1, translating a different open-reading frame and early stop codon, resulting in the shorter sequence. **C)** Cartoon organization of the C-tail exons (exon 15, 16, and 17) of the DCLK1

isoforms, comparing the translated protein sequence alignment.

188

189 Higher-order vertebrates have multiple isoforms of DCLK1 and DCLK2, where sequence variations occur
190 in either or both the N and C terminal regions attached to the kinase domain. Human DCLK1, for
191 example, has four unique isoforms. Isoforms 1 and 2 differ in C-terminal tail length due to variations in
192 exon splicing (**Figure 4A**). Further examination of the intron and exon boundaries indicates that human
193 DCLK1.1 contains an additional exon (exon 16) that is not spliced in DCLK1.2. Exon 16 is spliced with
194 exon 17 with a phase 2 intron, which introduces a shift in the reading frame and an earlier translated stop
195 codon (UGA) in exon 17 (**Figure 4B**). In DCLK1.2, exon 15 is spliced with exon 17, with a non-disruptive
196 phase 0 intron, resulting in the full translation of exon 17. These changes introduce multiple indels
197 (insertions and deletions) and result in the insertion of a phosphorylatable threonine (T688) (2) in
198 DCLK1.2 that is absent in the DCLK1.1 variant (**Figure 4B-C**), suggesting a possible exon duplication for
199 adaptive regulation of DCLK1 function by phosphorylation. DCLK1.2 is the best-characterized isoform in
200 terms of structure and function (26), and to compare it with DCLK1.1, we generated a series of C-terminal
201 tail deletion mutants to evaluate how variations in the C-terminal tail contribute to isoform specific DCLK1
202 functions.

203

204 **Isoform-specific variations encode changes in molecular dynamics, thermostability and catalytic**
205 **activity in DCLK1**

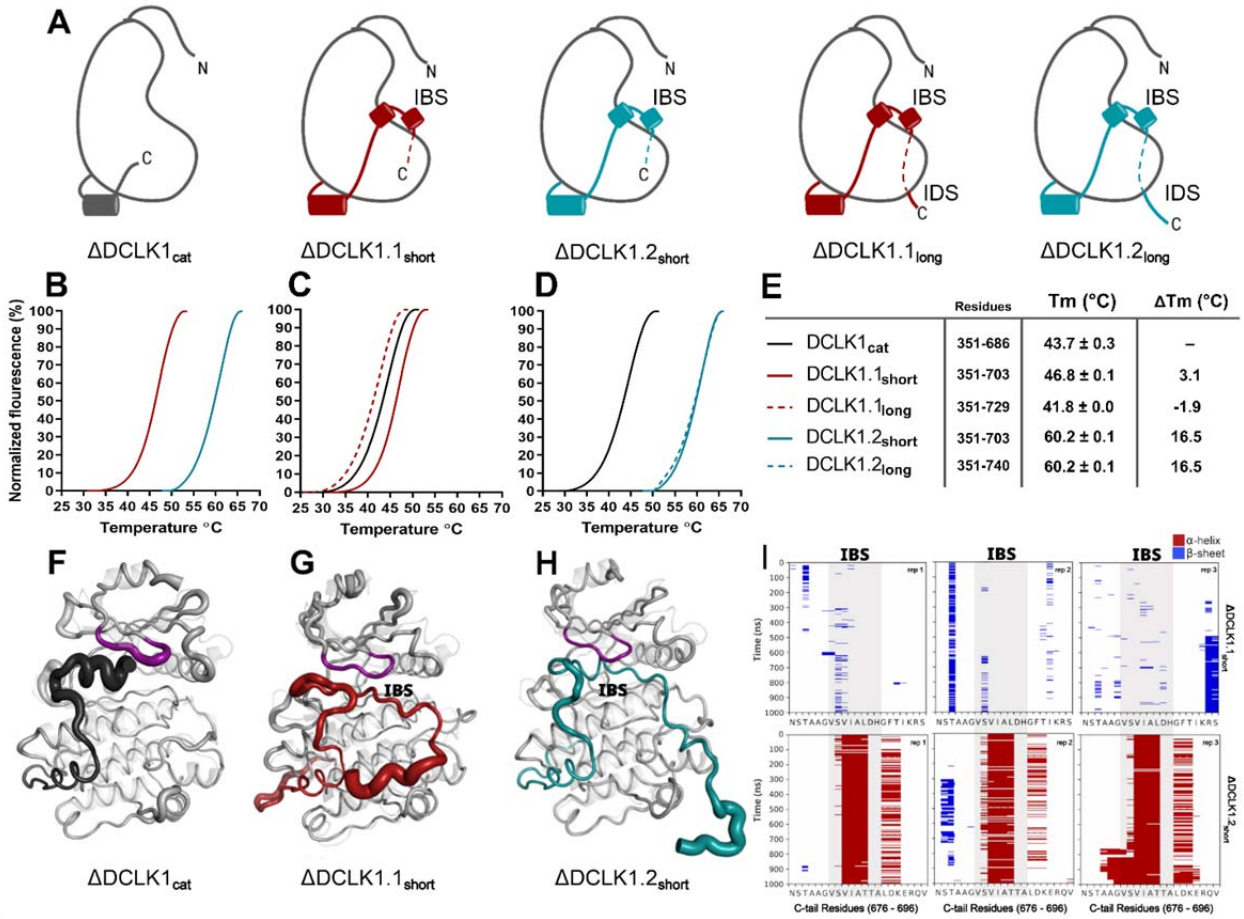

206

Figure 5: **A)** Cartoons of DCLK1 construct used in our assays, portraying the locations of the Inhibitory Binding Segment (IBS) and the Intrinsically Disordered Segment (IDS). **B-E)** DSF thermal denaturation profiling of the purified DCLK1 core catalytic domain, or tail-matched DCLK1.1 and DCLK1.2 proteins. Unfolding curves and changes in Tm values (ΔTm) for each protein relative to WT $DCLK1_{cat}$ are indicated. **F-H)** B-factor structural representations of $DCLK1_{short}$ proteins shown in A). The width of the region indicates the extent of flexibility based on averaged RMSF data from three one microsecond MD replicates. **I)** DSSP analysis of three replicates of one microsecond MD simulations showing the residues surrounding the IBS in the C-tail of $DCLK1.1_{short}$ and $DCLK1.2_{short}$. Blue indicates the presence of a Beta-sheet or Beta-bridge secondary structures and red indicates the presence of alpha-helical structures.

207
208 To study isoform specific differences in the C-tail, we employed experimental techniques to compare
209 protein stability and catalytic activity between purified DCLK1 proteins alongside molecular dynamics
210 simulations for DCLK1.1 and DCLK1.2 with different tail lengths. Isoforms 1.1 and 1.2 share identical
211 sequences across the kinase domain and within the first 38 residues of the C-tail, and we used this
212 information to design a new recombinant protein, termed $DCLK1_{cat}$ (residues 351-686). C-terminal to this
213 totally conserved region, both isoforms possess extended tail segments, which includes the putative

214 inhibitory binding segment (IBS; residues 682-688) and an additional intrinsically-disordered segment
215 (IDS; residues 703-end). To study the role of the C-tail in modulating kinase stability and activity, we
216 purified the DCLK1$_{cat}$, and C-tail containing (long and short) variants of each isoform, each of which lack
217 the N-terminal DCX domains (**Figure 5A**). SDS-PAGE demonstrated that protein preparations were
218 essentially homogenous after affinity and gel filtration chromatography (**Figure 5-figure supplement 1**).
219 The short forms of the recombinant proteins (DCLK1.1$_{351-703}$ and DCLK1.2$_{351-703}$) possess a partially
220 truncated C-tail and were designed to match the amino acid sequence previously used to solve the
221 structure of DCLK1.2 protein (26). Notably, these proteins exclude the IDS. The long forms of the DCLK1
222 proteins include the full-length C-tail for each isoform (DCLK1.1$_{351-729}$ and DCLK1.2$_{351-740}$) and incorporate
223 IDS domains. We first performed comparative thermal shift analyses to quantify variance in thermal
224 stability between the different purified proteins. When contrasting DCLK1.1$_{short}$ and DCLK1.2$_{short}$ which do
225 not differ in size or tail length but encode unique sets of amino acids in their partially truncated C-tail as a
226 result of alternative splicing (**Figure 4**), we observed that DCLK1.2 was some 14°C more stable than
227 DCLK1.1 (**Figure 5B**). When compared with DCLK1$_{cat}$, both DCLK1.1 short and long exhibited only subtle
228 changes in thermal stability (**Figure 5C & E**), whereas both DCLK1.2 proteins (DCLK1.2$_{short}$ and
229 DCLK1.2$_{long}$) were significantly stabilized (relative ΔTm >16°C, **Figure 5D & E**).
230
231 We next performed MD simulations to study the dynamics within the distinct DCLK1 C-tails that might
232 explain the observed difference in protein stability. The crystal structure of DCLK1.2 (pdb: 6KYQ) was
233 employed for the DCLK1.2$_{short}$ model and AlphaFold2 was used to model the other proteins (DCLK1$_{cat}$
234 and DCLK1.1$_{short}$). Comparison of the root mean square fluctuations (RMSF) of the two isoforms in three
235 different replicates of molecular dynamics simulations indicates strikingly different thermal fluctuations in
236 the C-terminal tails and catalytic domains (**Figure 5-source data 1**). In particular, the IBS segment
237 (between 682-688) is stably docked in the ATP binding pocket in DCLK1.2 and an alpha helical
238 conformation is maintained during the microsecond time scale across different replicates (**Figure 5I**,
239 bottom). In contrast, the IBS is more unstable in DCLK1.1, as indicated by high thermal fluctuations and a
240 lack of secondary structure propensity (**Figure 5I**, top). A caveat to bear in mind is that DCLK1.1 is an
241 AlphaFold2 model, which will also account for increased RMSF. Analysis of sequence variations and

structural interactions provides additional insights into the differential dynamics of the two isoforms. The helical conformation of the IDS in DCK1.2 is maintained during the simulation due, in part, to a capping interaction with Thr 687, which is absent in DCLK1.1 due to the alternative splicing event detailed above. Likewise, another key residue in DCLK1.2, Lys 692, anchors the tail to the catalytic domain through directional salt bridges with the conserved aspartates (Asp 511 and Asp 533) in the HRD and DFG motifs (**Figure 5, figure-supplement 2A**). These interactions are not observed in DCLK1.1 simulations because Lys 692 is substituted to a histidine (His 689), which is unable to form a corresponding interaction with the catalytic domain (**Figure 5, figure-supplement 2B**). These results indicate that the DCLK1.2 C-tail forms stable interactions with the kinase domain and kinase-specific motifs which drive the observed increase in thermal stability in our recombinant protein constructs (**Figure 5D**), while the more flexible DCLK1.1 C-tail forms fewer stable interactions with the kinase domain. This variable docking of the C-tail within the kinase domains of the two DCLK1 isoforms, and the extent to which this contributes to more transient or stable autoinhibited states was explored in more detail in the next section.

Figure 6:

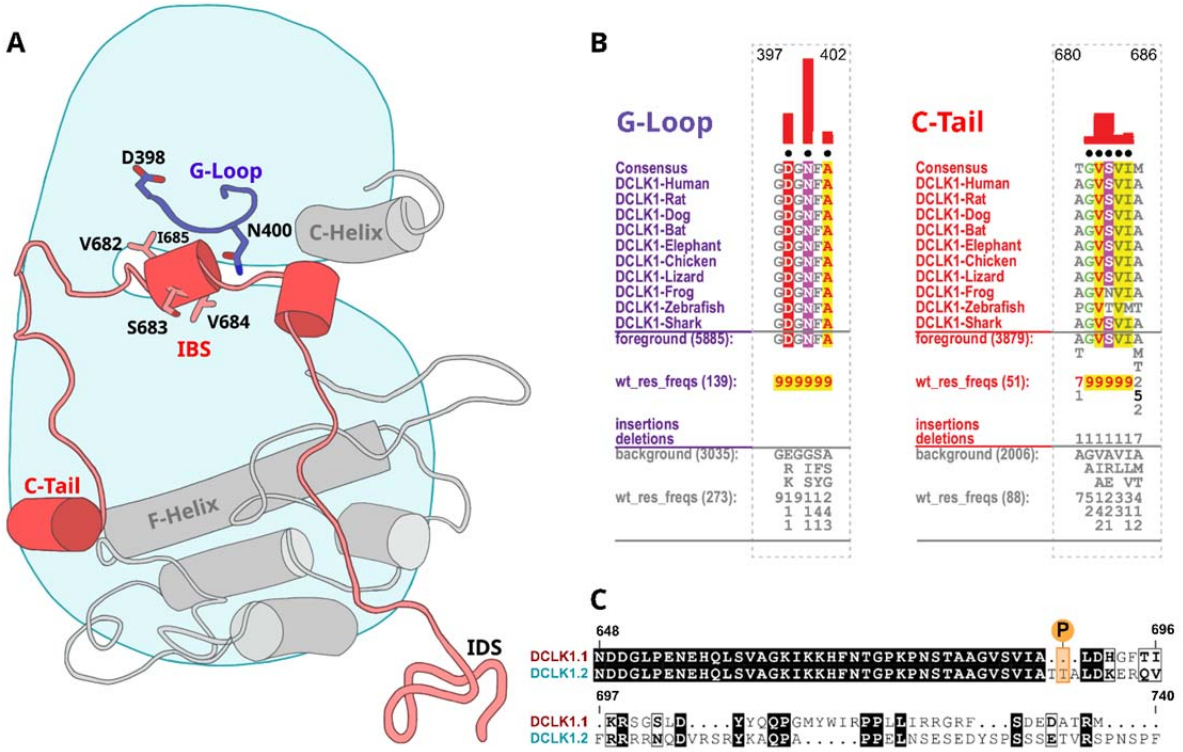

Figure 6: Identification of DCLK specific constraints. A) Cartoon of DCLK1.2 and the intrinsically disordered segment (IDS) with evolutionary constraints mapped to the kinase domain and C-tail. **B)**

Sequence constraints that distinguish DCLK1/2/3 sequences from closely related CAMK sequences are shown in a contrast hierarchical alignment (CHA). The CHA shows DCLK1/2/3 sequences from diverse organisms as the display alignment. The foreground consists of DCLK sequences while the background alignment contains related CAMK sequences. The foreground and background alignments are shown as residue frequencies below the display alignment in integer tenths (1–9). The histogram (red) indicates the extent to which distinguishing residues in the foreground diverge from the corresponding position in the background alignment. Black dots indicate the alignment positions used by the BPPS (Neuwald, 2014) procedure when classifying DCLK sequences from related CAMK sequences. Alignment number is based on the human DCLK1.2 sequence (UniProt ID: O15075-2). **C)** Sequence alignment of human DCLK1 isoforms.

Residues contributing to the co-evolution and unique tethering of the C-terminal tail to the DCLK catalytic domain.

To identify specific residues that contribute to the unique modes of DCLK regulation by the C-terminal tail, we performed statistical analysis of the evolutionary constraints acting on DCLK and related CAMK family sequences. We aligned the catalytic domain of DCLK and related CAMK sequences from diverse organisms and employed the Bayesian Partitioning with Pattern Selection (BPPS) method (30) to identify residues that most distinguish DCLK sequences (foreground alignment in **Figure 6B**) from CAMK sequences (background alignment). Beyond the catalytic domain, DCLKs share sequence and structural similarities in the first helix of the tail (αR1 in CAMK1) (31,32), with other CAMKs but share no detectable sequence similarity beyond this helical segment. DCLKs also share a CAMK-specific insert segment located between F and G helices in the catalytic domain, although the nature of residues conserved within the insert is unique to individual CAMK families (**Figure 6-figure supplement 1**). BPPS analysis revealed DCLK-specific constraints in different regions of the kinase domain, most notably, the ATP binding G-loop, N terminus of the C-helix, the activation loop, and C-terminus of the F-helix (**Figure 6-figure supplement 2**).

Some of the most significant DCLK specific residue constraints map to the ATP binding G-loop (GDGNFA motif) (Figure 6A-B). In particular, Asp 398, Asn 400 and Ala 402 are unique to DCLKs as the corresponding residues are strikingly different in other CAMKs. Asp 398 is typically a charged residue (K/R) in other CAMKs while Asn 400 and Ala 402 are typically hydrophobic and polar residues, respectively (see residues frequencies in background alignment; **Figure 6B**). Notably, both Asn 400 and Asp 398 make direct interactions with residues in the C-tail either in the crystal structure or molecular dynamics simulations (see below). Likewise, DCLK conserved residues in the C-helix and activation loop

tether the C-terminal tail to functional regions of the kinase core, suggesting co-option of the DCLK catalytic domain to uniquely interact with the flanking cis regulatory tail.

Figure 7:

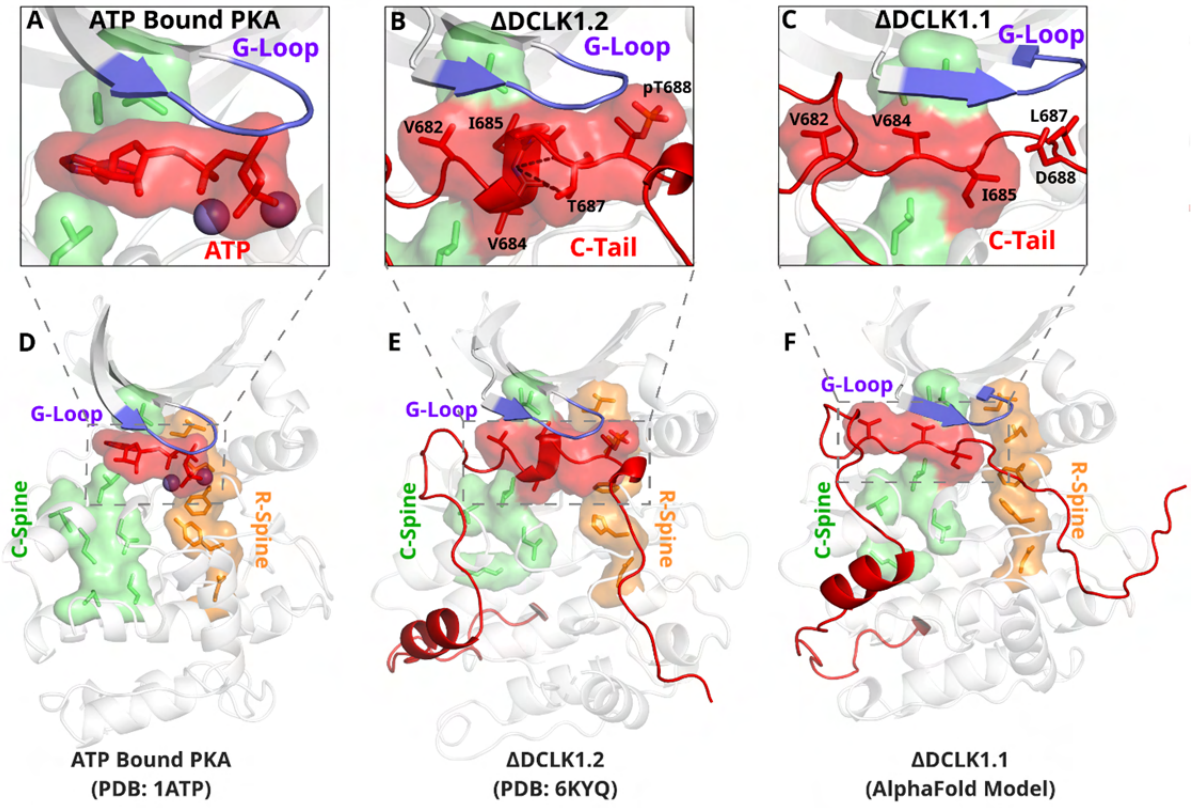

Figure 7: The DCLK1 C-tail 'completes' the regulatory C-spine (green). A) PKA crystal structure (pdb: 1ATP) with bound ATP in red and Mg^{2+} in purple. The C-spine is completed by the adenine ring of ATP. The gamma phosphate of ATP hydrogen bonds with the second glycine of the G-loop. **B)** DCLK1.2 crystal structure (pdb: 6KYQ) showing how the C-tail (red) docks underneath the pocket and mimics the ATP structure. The C-spine is completed by V682 and V684 in the C-tail and helical segments defined using DSSP are shown. T687 is also depicted making multiple hydrogen bonds with the backbone of V684 and I685 (dashed lines). **C)** DCLK1.1 AlphaFold2 model showing an unstructured loop in the C-tail docking into the ATP binding pocket, where V684 and I685 are predicted to complete the C-spine. The average per-residue confidence of the C-tail is 49%. **D-F)** Zoomed out versions of A-C, demonstrating how the DCLK1 C-tail docks into the ATP binding cleft, akin to ATP in PKA.

An autoinhibitory ATP-mimic completes the C-spine and mimics the gamma phosphate of ATP.

The most stable segment of the C-tail based on the B-factor and RMSF fluctuations in MD simulations is a unique region (682-688 in DCLK1.2) that docks into the ATP binding pocket through both hydrophobic and hydrogen-bonding interactions. Remarkably, this peptide segment mimics the physiological ATP

292 ligand, and stabilizes the catalytic domain through ‘completion’ of the hydrophobic catalytic spine (**Figure**
293 **7A**, (33)). The residues that mimic adenosine and complete the C-spine of DCLK1 are Val 682, Val 684,
294 and Ile 685 (PDB: 6KYQ), which are part of the α-helix that docks to the ATP-binding pocket (**Figure 7B**).
295 Interestingly, based on our BPPS analyses, these C-tail residues are uniquely vertebrate DCLK1-specific
296 pattern constraints. At the tail end of this α-helix are two Thr residues, Thr 687 and Thr 688. As previously
297 noted, these Thr residues mark the beginning of exon 17, and are one of the key variations between
298 human DCLK1 isoforms, found only in DCLK1.2 variants.
299
300 Structural analysis and MD simulations reveal that Thr 687 in DCLK1.2 caps the stable α-helix that
301 extends the C-spine (**Figure 7B, Figure 7-figure supplement 1B**). In comparison, the same region in
302 DCLK1.1, which lacks Thr 687, is predicted to be unstructured. Upon phosphorylation, Thr 688 in
303 DCLK1.2 can mimic the gamma phosphate of ATP by maintaining a stable hydrogen bonding distance
304 with the backbone of the second glycine of the G-loop (G399) (**Figure 7B**, **Figure 7-figure supplement**
305 **1C**). We additionally observe that the sidechain of Asn 400, a DCLK-specific G-loop constraint, further
306 stabilizes the phosphate group in pThr 688 through hydrogen bonding. As previously mentioned, Thr 688
307 is unique to DCLK1.2. The lack of this functional site in DCK1.1 is correlated with increased RMSF and
308 instability of the ATP-mimic segment in isoform 1 MDs (**Figure 5C-D, Figure 7-figure supplement 1B**).
309 Comparatively, MD analysis of DCLK1.2 and a phosphothreonine-containing DCLK1.2 demonstrates
310 reduced C-tail fluctuations, suggesting the potential regulatory involvement of Thr 688 phosphorylation for
311 further modulation of the autoinhibited conformation (**Figure 7-figure supplement 1C**), consistent with
312 previous findings (2).
313

Figure 8:

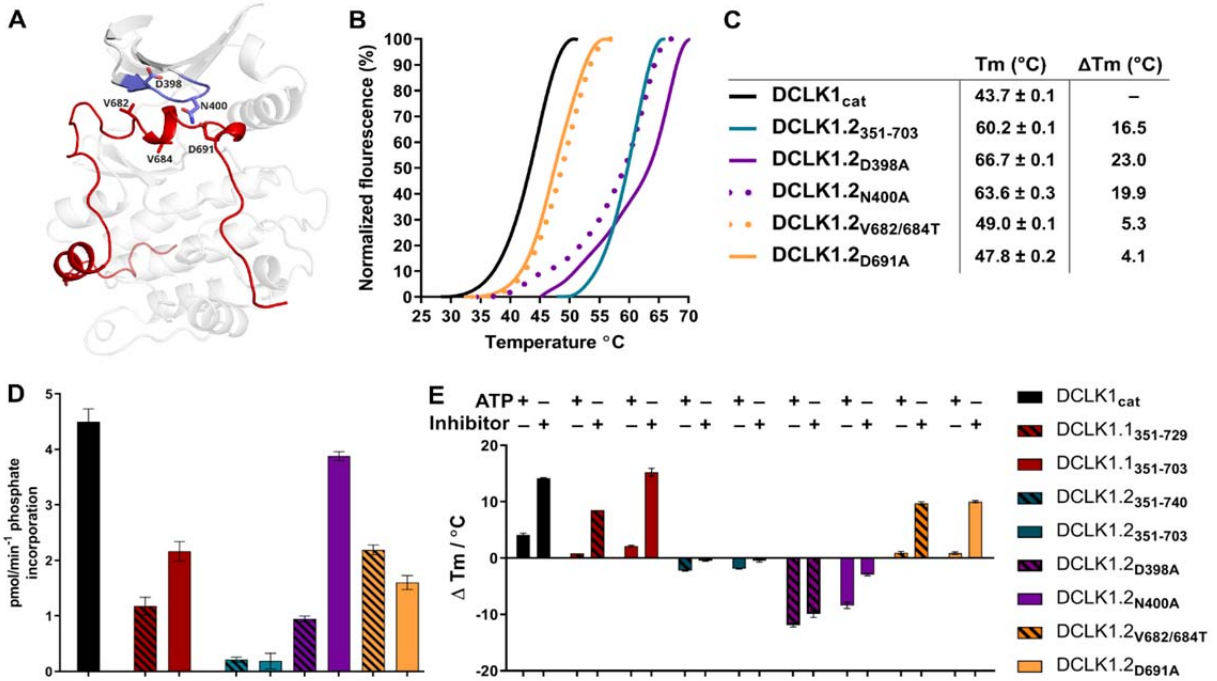

Figure 8: A) Structural depiction of DCLK1.2 (PDB: 6KYQ) showing the location of modified DCLK1 amino acids on the G-loop (purple) or C-tail (red). **B-C)** Differential Scanning Fluorimetry assays depicting thermal denaturation profiles of each protein along with the calculated Tm value. **D)** Kinase assays. DCLK1-dependent phosphate incorporation (pmol/min^{-1}) into the DCLK1 peptide substrate was calculated for DCLK1$_{cat}$, long and short DCLK1.1 and the indicated DCLK1.2 variants. **E)** Thermal stability analysis in the presence of ATP or DCLK1-IN-1 for DCLK1 proteins. For DCLK1.2, all proteins were generated in the DCLK1.2 short background.

Mutational analysis support isoform-specific allosteric control of catalytic activity by the C-terminal tail.

To evaluate how sequence differences between DCLK1.1 and DCLK1.2 affected both thermal stability and catalytic potential, we generated targeted mutations at contact residues within the Gly-rich loop and C-tail of DCK1.1 and DCLK1.2 (at the indicted residues depicted in **Figure 8A**) which we predicted would disrupt or destabilize C-tail docking within the domain. All proteins were purified to near homogeneity by IMAC and size exclusion chromatography filtration (**Figure 5-figure supplement 1**), and the thermal stability of a panel of DCLK1.2 mutant and WT proteins were compared side-by-side with the DCLK1$_{cat}$ (**Figure 8B**). The ΔTm values obtained (**Figure 8C**) demonstrate that mutation of Asp 398 or Asn 400 in the Gly-rich loop are by themselves insufficient to destabilize DCLK1.2. In marked contrast, dual mutation of the hydrophobic pair of Val 682 and Val 684 residues to Thr, or mutation of the acidic tail residue Asp691, resulted in a pronounced reduction in DCLK1.2 thermal stability. Moreover, the recorded Tm

330 values for these latter two mutations quite closely resembled the Tm of $DCLK1_{cat}$ (which lacks the C-tail
331 entirely), which is consistent with the uncoupling of the C-tail and a commensurate decrease in thermal
332 stability associated with loss of this interaction. We next determined the catalytic activity of all our
333 recombinant DCLK1.1 and DCLK1.2 proteins side-by-side (**Figure 8D, Figure 8-figure supplement 1B**).
334 Although partially diminished in relation to $DCLK1_{cat}$, both $DCLK1.1_{short}$ (351-703) and $DCLK1.1_{long}$ (351-
335 729) variants possess robust catalytic activity. This suggested ineffective ATP-competitive auto-inhibition
336 mediated by the C-tail segment of DCLK1.1 and is consistent with their closely matched Tm values to
337 $DCLK1_{cat}$ (**Figure 5C**). In marked contrast, detectable kinase activity for short (351-703) or long (351-740)
338 DCLK1.2 proteins was significantly blunted compared to $DCLK1_{cat}$, exhibiting just ~5% of the activity of
339 the catalytic domain alone. We also utilized autophosphorylation as a proxy for overall kinase activity.
340 Quantitative tandem mass spectrometry (MS/MS) analysis of site-specific autophosphorylation within
341 $DCLK1.1_{short}$ and $DCLK1.2_{short}$ confirmed a marked reduction in the site-specific abundance of phosphate
342 in DCLK1.2 when compared to DCLK1.1 at two distinct sites that could be directly and accurately
343 quantified (Ser 438 and Ser 660, relative abundance set to 1, **Figure 8-figure supplement 1A**).
344 Unfortunately, we were unable to assign site-specific Thr 688 phosphorylation in DCLK1.2, since it
345 resides in a large, multiply phosphorylated tryptic peptide with multiple potential sites of phosphorylation.
346 Furthermore, quantitative abundance calculations between the two isoforms was not possible since Thr
347 688 is absent in DCLK1.1. Interestingly, amino acid substitutions in the G loop or the C-tail of DCLK1.2
348 designed to subvert C-tail and ATP site interactions also had major effects on DCLK1.2 catalytic activity.
349 DCLK1.2 D398A was activated some 5-fold when compared to the WT form, whereas DCLK1.2 N400A
350 was almost as active as the $DCLK1_{cat}$. Consistently, DCLK1.2 V682T/V684T and D691A proteins were
351 also much more active than the WT form of DCLK1.2 (**Figure 8D**, see **Figure 8-figure supplement 1B**
352 for kinetic analysis). Moreover, quantitative MS/MS analysis of purified DCLK1.2 D398A, N400A and
353 V682T/V684T proteins demonstrated that Ser 438 and (especially) Ser 660 autophosphorylation sites
354 increased in abundance, consistent with the enhanced activity of these proteins compared to WT
355 DCLK1.2 (**Figure 8-figure supplement 1C**). Together, these observations confirm that these targeted
356 mutations are sufficient to relieve ATP-competitive C-tail autoinhibition by physical tail uncoupling; this

357 model is also strongly supported by marked changes in the thermal stability of the mutant proteins,
358 particularly for V682/684T and D691A (**Figure 8B**).
359 To expand on this finding, we investigated the interaction of Mg:ATP or DCLK1-IN-1 to our panel of
360 DCLK1.1 and 1.2 proteins (**Figure 8E**), using changes in thermal stability as a reporter of ligand binding.
361 DCLK1$_{\mathbf{cat}}$ (351-686), DCLK1.1$_{short}$ (351-703) and DCLK1.1$_{long}$ (351-729) proteins all behaved similarly in
362 the presence of either Mg:ATP or DCLK1-IN-1, inducing marked stabilization. In contrast, DCLK1.2$_{short}$
363 (351-703) or DCLK1.2$_{long}$ (351-740) proteins registered negligible thermal shifts in the presence of the
364 same concentration of either ligand, which is in-line with the C-tail tightly occupying the ATP-binding site
365 and obstructing their binding. Remarkably, D398A and N400A DCLK1.2, whose high basal Tm values
366 (compared to DCLK1$_{cat}$) are consistent with stabilization by docking of the C-tail within the kinase domain,
367 were markedly destabilized in the presence of either ligand. This suggests that incorporation of these G-
368 loop mutations in isolation is insufficient to dislodge the C-tail, but rather that the stability of the interaction
369 is compromised to the extent that either ATP or DCLK-IN-1 can competitively dislodge the bound tail from
370 the ATP active site, resulting in a net destabilization caused by lack of tail engagement. This observation
371 is corroborated by the results of our kinase assays, where both D398A and N400A mutants were more
372 active than WT DCLK1.2, confirming appropriate ATP binding (a pre-requisite for catalysis). Finally,
373 DCLK1.2 V682T/V684T and D691A, which exhibit lower basal Tm values than the WT protein (indicating
374 a loss of tail interaction), were both stabilized in a ligand-dependent manner to a similar degree to that
375 observed for DCLK1$_{cat}$ and DCLK1.1 proteins (**Figure 8E**). Collectively, these observations clearly
376 demonstrate that the C-tail section of DCLK1.2 can both stabilize the canonical DCLK kinase domain and
377 inhibit kinase activity (by impeding the binding and structural coordination of Mg:ATP) much more
378 effectively than that of DCLK1.1. Our targeted mutational analysis of key contact residues in DCLK1.2
379 also clearly shows that this is a consequence of specific amino acid interactions that are absent in
380 DCLK1.1 due to alternative-splicing sequence deviations.
381
382 **Classification of DCLK regulatory segments.**
383 We synthesized our experimental findings by classifying the DCLK C-tail into six functional segments,
384 based on interactions with different regions of the catalytic domain and their conservation between the C-

385 tail splice variants we analyzed (**Figure 9**): First is an ATP-mimetic peptide segment (residues 682-688 in
386 DCLK1.2) that readily mimics physiological ATP binding by completing the C-spine in the nucleotide-
387 binding site. The inhibitory peptide also contains a phosphorylatable Thr residue, which sits adjacent to
388 the highly characteristic Gly-rich loop (GDGNFA, residues 396-402). Second, we define a
389 pseudosubstrate mimic (PSM, residues 692-701), which interacts with the acidic HRD and DFG Asp side-
390 chains and docks in the substrate pocket occluding substrate access. Third, at the C-terminus of the tail,
391 lies an intrinsically disordered segment (IDS, residues 702-749, **Figure 9-figure supplement 1**), which
392 packs dynamically against DCLK conserved residues in the kinase activation loop. Fourth, at the
393 beginning of the C-tail lies a CAMK-tether (residues 654-664), a set of residues that pack against a
394 CAMK-specific insert in the C-lobe. In many CAMK crystal structures, this insert makes multiple contacts
395 with the F-helix and C-tail (**Figure 6-figure supplement 1**). Fifth, this is followed by a highly dynamic
396 pseudosubstrate region (residues 672-678) that occludes the substrate pocket and will thus interfere with
397 substrate phosphorylation. Sixth, a transient beta-strand is formed in DCLK1.2 through amino acid
398 specific sequences that help modulate and potentially strengthen binding of the C-tail in this isoform
399 (**Figure 7-figure supplement 1A-B**). Collectively, these segments and their associated interaction sites
400 demonstrate that co-evolution of the unique C-tail with the catalytic domain is the central hallmark of
401 DCLK functional divergence, and that changes in these segments possess the ability to 'supercharge'
402 catalytic output of the kinase. The combinatorial diversity of events that modulate C-tail function may
403 allow DCLKs to maintain a nimble balance between various tasks including ATP-binding, substrate-based
404 phosphorylation, coordination of DCX domain phosphorylation and structural disposition, kinase
405 autoinhibition and allosteric regulation. Additionally, differences in cellular localization (e.g. cytoplasm or
406 nucleoplasm) and tissue-specific expression may enable contextual DCLK regulation through these
407 modular sequence segments.
408

Figure 9:

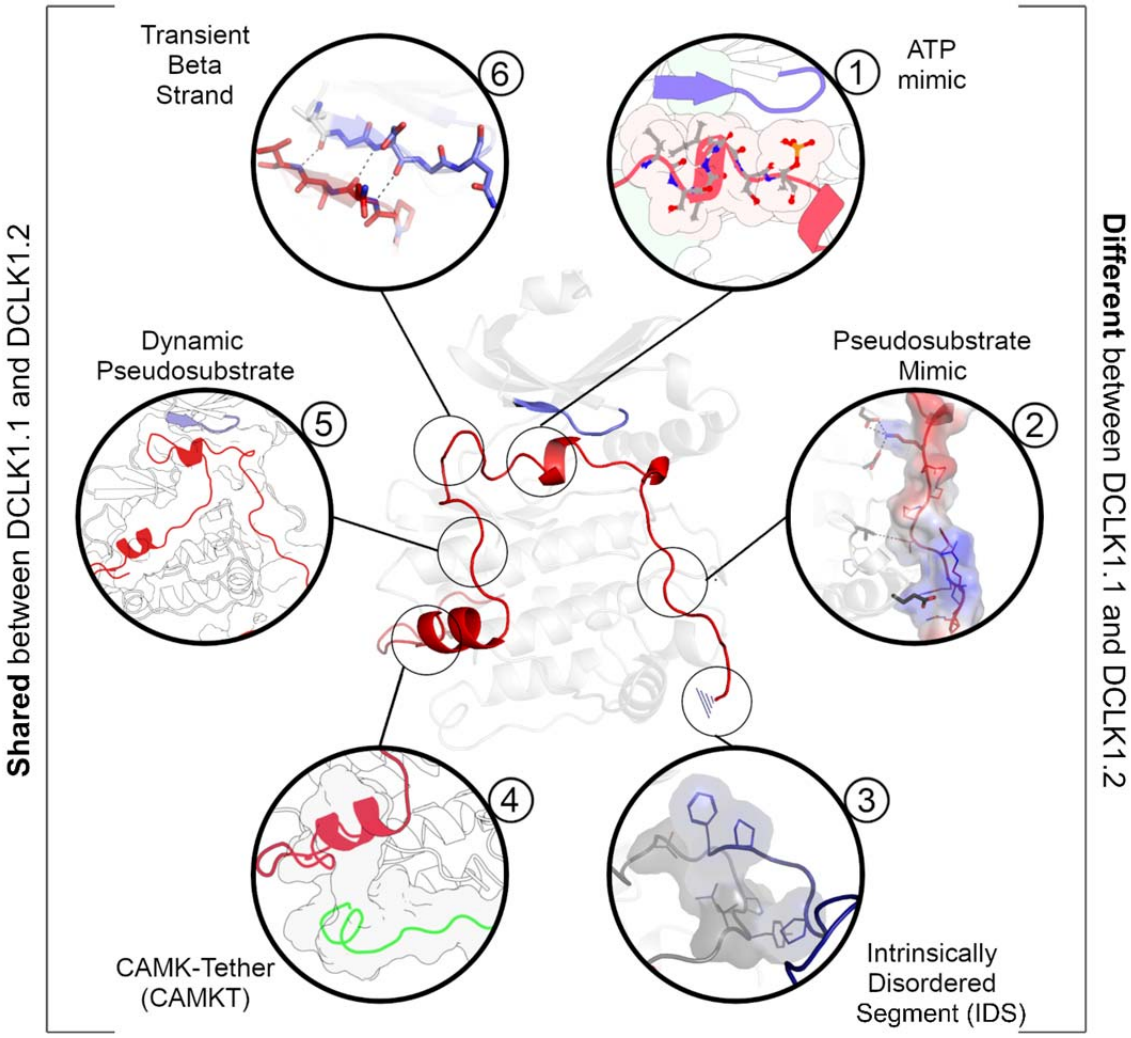

Figure 9: A DCLK1 C-tail can act as a multi-functional Swiss Army Knife, using six distinct segments for a variety of regulatory functions including mimicking ATP binding/association, stabilizing the G-loop, occluding the substrate binding pocket, and packing against the kinase activation loop.

411 # Discussion
412
413 The kinase domain is a conserved switch for phosphorylation-based catalytic regulation. Yet the
414 complexity of cell signaling pathways demands other nuanced forms of regulation beyond binary "on" or
415 "off" switch-based mechanisms. For many Ser/Thr kinases, including AGC and CAMK families, these
416 distinct regulatory functions come from segments which flank the kinase domain, N- and C-terminal
417 regions, which serve to modulate activity through allosteric activation, inhibition, or rheostatic behaviors
418 that change based on environmental conditions (4). In this study, we expand on our knowledge of
419 allosteric diversity in the human kinome by revealing how alternative splicing of the DCLK1 C-tail
420 contributes to isoform-specific behaviors, coupling regulation of catalytic output, phosphorylation, protein
421 dynamics and stability, substrate binding, and protein-protein interactions. Our "Swiss Army Knife" model
422 for DCLK1 expands our view of allosteric regulation as not just a dynamic process facilitated by proteins,
423 but one where adaptive genetic mechanisms, like differential splicing, dexterously tune isoform-specific
424 functions for specific cellular signaling roles; in the case of DCLK1.1, this allows 'supercharging' of
425 catalysis between splice variants due to key amino acid differences in the C-tail that are lacking in the
426 DCLK1.2 isoform.
427 Multiple members of the human kinome have independently evolved C-tail regions that dock to the N or
428 C-lobe of the kinase domain *in cis*. In the case of the AGC kinases, the C-terminal tail is a very well-
429 studied *in-cis* modulatory element that serves to explain a variety of regulatory properties in this kinase
430 sub-family (14,34–36). Classical deletion studies with members of the CAMK family, have also revealed a
431 cis-acting inhibitory element lying C-terminal to the catalytic domain of both CAMK1 (37) and CAMK2
432 (38). More recent examples of the diversity of C-tail function in CAMK family members are presented by
433 the human pseudokinases TRIB1 and TRIB2, which employ C-tail sequences to either latch (and
434 structurally restrict) the atypical kinase domain or to bind competitively to the Ubiquitin E3 ligase COP1
435 (39,40). Functional disengagement of the TRIB1 or TRIB2 tail through deletion, mutagenesis or small
436 molecule binding has marked effects on pseudokinase conformation, intrinsic stability and cellular
437 transformation (41–44).
438

439

440

441 **A novel pseudosubstrate region encoded by DCLK1.**

442 In addition to the marked differences between DCLK1 splice variants relevant to nucleotide binding, small
443 molecule interactions and catalysis, our work also reveals two unique pseudosubstrate segments present
444 before and after the IBS. Before the IBS segment, we observe the formation of an anti-parallel transient
445 beta sheet with the beta1 strand in the catalytic domain (**Figure 5I**, **Figure 7-figure supplement 1A-B**).
446 During the formation of this transient structure, the C-tail dynamically occludes part of the substrate
447 binding pocket. A beta-sheet is observed in all three MD replicates of DCLK1.1, but only in a single
448 replicate of DCLK1.2 dynamic analysis. At the other end of the IBS is another pseudosubstrate segment
449 whose structure and dynamics change as a result of alternative exon splicing. In DCLK1.2, the
450 pseudosubstrate segment is stable, with an average RMSF of 1.8 Angstroms, facilitated by key
451 interactions from Lys 692, which coordinates acidic residues in the HRD and DFG motifs (**Figure 5-figure**
452 **supplement 2A**). In DCLK1.1, Lys 692 is replaced by a His, which weakly coordinates with the HRD and
453 DFG motifs, resulting increased dynamics of the segment and an RMSF of 3.1Å (**Figure 5**, **Figure 5-**
454 **figure supplement 2B**). Together, residue variation between isoforms contribute to differences in stability
455 and alteration of dynamics of the tail. HPCAL1 was recently proposed as a possible substrate that
456 activates DCLK1 in a calcium-dependent manner, but it is unclear how it may bind DCLK1 (26). Because
457 only exon 15 of the C-tail is conserved between the isoforms, it is possible the location of binding occurs
458 in this dynamic pseudosubstrate segment prior to the IBS, where increased flexibility and occlusion of the
459 substrate pocket is reflective of the absence of HPCAL1, or a similar calmodulin-like substrate.

460

461 **Discovery of the DCLK1 ATP-Mimic region; a splice-variant specific regulatory module.**

462 Our structural analysis of DCLK1 reveals a remarkable structural mimic of ATP located in the C-tail, which
463 differs markedly between DCLK1.1 and DLCK1.2 splice variants. We note for the first time that a set of
464 three residues in the ATP-mimic, Val 682, Val 684, and Ile 685, are conserved across all isoforms of
465 DCLK1 and DCLK2 (Figure 1C) and serve to extend the kinase C-spine. Mutation of these residues in
466 DCLK1.2 uncouples tail binding and activates the kinase. Proximal to these residues are two Thr residues

467 (Thr 687 and Thr 688) ,which are only found in DCLK1.2. Based on proteomics data, both Thr residues
468 can be phosphorylated (2) and are thus likely to be regulatory in DCLK1.2. By analyzing DCLK1
469 dynamics using MD simulations, we observed multiple key interactions between the G-loop and the C-tail
470 in DCLK1, the most critical of which appear to be dipole interactions with the second glycine in the G-loop
471 by the phosphothreonine. In addition, Thr 687 contributes to increased stabilization of DCLK1.2 tail by
472 forming a C-cap with the helical ATP-mimic segment. We aligned the intensively-studied protein kinase
473 (PKA, pdb: 1ATP), a DCLK1.2 structure (pdb: 6kyq), and frames of our MD trajectory, which demonstrate
474 remarkable overlap of the ATP gamma phosphate and C-tail phosphothreonine, which seemingly acts as
475 a mimic for the ATP co-factor. As phosphorylation is reported to lead to DCLK1 inhibition, this suggests a
476 complex mechanism of regulation, in which the DCLK-specific constraints in the G-loop, the intrinsic
477 flexibility of the C-tail, and threonine phosphorylation, by cis or trans-mediated modification, systematically
478 prevent hyperphosphorylation of the doublecortin domains and cellular effects.
479 Finally, we have evaluated the terminal residues in the DCLK1 C-tail, which are predicted to be
480 intrinsically disordered. Side-by-side analysis of DCLK1.1 and DCLK1.2 in which this region is added from
481 a common core terminating at residue 703, shows that increasing the length of the tail in both DCLK1.1
482 and DCLK1.2 has little additional effect on the inhibitory or stabilizing effects driven by the highly ordered
483 tail regions that precede it. Kinase domains are regulated by IDRs in a multitude of ways, but the CAMK
484 family is specifically enriched for adapted C-terminal extensions that, as we show here, can block the ATP
485 and substrate binding, and enzymatically inactivate the kinase domain by occlusion of the activation loop
486 through a flexible helical IDS on their C-tail (4). We note that the DCLK1.2 kinase domain crystallizes in
487 an 'active' closed conformation, despite binding of the C-tail in an autoinhibitory manner (26). Repeated
488 packing motions of the IDS against the activation loop in all replicates of DCLK1.1 MD simulations,
489 suggest that tail may occlude the activation loop, similar to other CAMKs, possibly pointing to a mode of
490 *cis* autoregulation. Conversely, AlphaFold2 predicts the placement of the DCX domains as adjacent to the
491 IDS in both DCLK1.1 and DCLK1.2 (Figure S1). It is possible, like other CAMKs, the IDS helps facilitate
492 protein binding, whether to the DCX domains, calcium-modulated proteins, or other kinases.

493 **Evolutionary divergence and functional specialization of DCLKs**

494 For the DCLK family as a whole, we discovered phylogenetic divergence between DCLK1 and 2 as a
495 relatively recent event, (Figure 1A) in which metazoan DCLK3 is the more ancestral DCLK gene from
496 which DCLK1 and 2 emerged after duplication. Because of shared evolutionary constraints and the recent
497 divergence between DCLK1 and 2, we surmise the functional specialization of the DCLK1 tail is shared
498 between these paralogs. Moreover, for the first time, we quantify key differences between human
499 DCLK1.1 and 1.2 isoforms in the C-tail that can be reversed by amino acid changes. The differences
500 between isoforms 1 and 2 are generated by variations in exon splicing, which change both the C-tail
501 protein sequence, and introduce or exclude potential phosphorylation sites. Expression of the highly
502 autoinhibitable DCLK1.2 isoform is believed to be predominant during the brain in embryogenesis, and
503 DCLK1.1 is also thought to be present in the adult brain (45). It is therefore possible that an altered ratio
504 in DCLK1.1/1.2 expression, accompanied by changes in the requirement for DCLK1 auto-regulation, are
505 relevant for early neurogenesis. The overall sequence similarity at the protein level, despite the loss of a
506 putative phosphorylation site, suggests a possible exon duplication in the C-tail where polymorphisms
507 allow for adaptive regulation during development and proliferation. Indeed, we speculate that the induced
508 expression of DCLK1.2 splice variants in multiple cancer subtypes (46) is likely to be indicative of a
509 survival and drug-resistance role that could be targetable with new types of small molecule. Although
510 nanomolar DCLK1 ATP-site inhibitors such as DCLK1-IN-1 have been developed that can bind tightly to
511 the DCLK1 ATP site (**Figure 3** and **Figure 3-figure supplement 1**), the problematic existence of human
512 DCLK1.1 and DCLK1.2 splice variants with their distinct auto-inhibitory properties, may present a
513 challenge to compound engagement in the cell, where relief of auto-inhibition through C-tail undocking in
514 DCLK1.2 is likely to require a high concentration of compound in order to compete and disengage
515 interactions at the ATP site. Indeed, although potent chemical DCLK1 inhibitors such as DCLK1-IN-1 are
516 known to influence DCLK1 autophosphorylation and cell motility, they have relatively modest effects in
517 cells in terms of cytotoxicity (29,47). Therefore, we propose that the dual inhibitory effects of the C-tail
518 and the transmission of this information to adjacent DCX domains, which control adaptive cellular
519 phenotypes such as EMT in cancer cells (48), may make allosteric classes of DCLK1 inhibitor a preferred
520 therapeutic option, especially if they can be tailored specifically towards DCLK1.1 or DCLK1.2, whose
521 autoregulation is different in terms of the varied molecular details we uncover here.

522

Materials and Methods

Ortholog Identification. To identify orthologs, we used the software KinOrtho (49) to query one-to-one orthologous relationships for DCLK1/2/3 across the proteome. After collation of the various orthologs, we parsed the sequence data for taxonomic information and classified each sequence by family. We further separated human DCLK1 into each unique isoform and aligned them.

Phylogenetic Analysis. We identified diverse DCLK orthologs from the UniProt database (50) using an profile-based approach (51). From this dataset, we manually curated a taxonomically diverse set of DCLK orthologs composed of 36 sequences spanning 16 model organisms. These sequences were used to generate a maximum-likelihood phylogenetic tree using IQTREE version 1.6.12 (52). Branch support values were generated using ultrafast bootstrap with 1000 resamples (53). The consensus tree was selected as the final tree. The optimal substitution model for our final topology was determined to be LG (54) with invariable sites and discrete gamma model (55) based on the Bayesian Information Criterion as determined by ModelFinder (56). We rooted our final tree against an outgroup of 17 closely related human CAMK kinases using ETE Toolkit version 3.1.2 (57).

Sequence and Structure Analysis. MAFFT (58) generated multiple sequence alignments were fed into the Bayesian Partitioning with Pattern Selection (BPPS) tool to determine evolutionarily conserved and functionally significant residues (30). Constraints mapped onto AlphaFold-predicted structures were visualized in PyMOL to analyze biochemical interactions.

Rosetta Loop Modeling. Loop modeling was performed on the crystal structure (6KYQ) using the Kinematic Loop Modeling protocol (59) to model missing residues. Following this, the structure underwent five cycles of rotamer-repacking and minimization using the Rosetta Fast-relax protocol (60).

DSSP Analysis. To analyze changes in secondary structure over our MDs, we employed the DSSP command in GROMACS. This produces an output that contains an array of secondary structure values against each residue. The MDAnalysis python module (61) was used to plot these values.

Molecular Dynamics. PDB constructs were generated by retrieving structural models RCSB and the AlphaFold2 database. Post-translational modifications were performed in PyMOL using the PyTMs plugin. All structures were solvated using the TIP3P water model (62). Energy minimization was run for a maximum of 10,000 steps, performed using the steepest-descent algorithm, followed by the conjugate-gradient algorithm. The system was heated from 0K to a temperature of 300K. After two equilibration steps that each lasted 20 picoseconds, 1 microsecond long simulations were run at a two femtosecond timestep. Long-range electrostatics were calculated via particle mesh Ewald (PME) algorithms using the

559 GROMACS MD engine (63). We utilized the CHARMM36 force field (64). The resulting output was
560 visualized using VMD 1.9.3 (65). All molecular dynamics analysis was conducted using scripts coded in
561 Python using the MDAnalysis module (61).
562
563 **Computational Mutational Analysis**. Cartesian ddG in Rosetta (66) was utilized to predict potential
564 stabilizing and destabilizing mutations in the enzyme structure. We performed three replicates per
565 mutation and averaged the Rosetta energies. All mutant energies were then subtracted by the wt Rosetta
566 energy to generate a panel of ddG values relative to wt. Combined with our sequence analyses, we
567 mutated kinase and DCLK-specific constraints to identify destabilizing interactions in the c-tail.
568
569 **Exon-Intron Boundary Mapping.** The precise gene structure of DCLK1 isoforms were mapped onto the
570 human genome with each isoform used as a query protein sequence in order to generate exon-intron
571 borders. This was achieved using Scipio (version 1.4.1) (67) with default settings. Exons were numbered
572 based on Ensembl annotations (68). The translation of each annotated gene sequence to protein
573 sequence was provided with the output file (**Figure 4-source file 1-4**).
574
575 **DCLK1 cloning and recombinant protein expression.** 6His-DCLK1 catalytic domain (351-686),
576 DCLK1.1 351-703 (short C-tail) or 351-729 (full C-tail), DCLK1.2 351-703 (short C-tail) or 351-740 (full C-
577 tail), and DCLK1.2 351-703 containing D398A, N400A, V682T/V684T or D691A substitutions were
578 synthesized by Twist Biosciences in pET28a. 6His-GST-(3C) DCLK1.1 351-689 was amplified PCR and
579 cloned into pOPINJ. Kinase dead, D533A 6His-GST-(3C) DCLK1.1 351-689 was generated by PCR-
580 based site directed mutagenesis (**Figure 3-source data 3**). All plasmids were sequenced prior to their
581 use in protein expression studies. All proteins, including 6His-GST-(3C) DCLK1 351-689, with a 3C-
582 protease cleavable affinity tag, were expressed in BL21(DE3)pLysS *E. coli* (Novagen) and purified by
583 affinity and size exclusion chromatography. The short N-terminal 6-His affinity tag present on all other
584 DCLK1 proteins described in this paper was left in situ on recombinant proteins, since it does not appear
585 to interfere with DSF, biochemical interactions or catalysis.
586
587 **Mass Spectrometry.** Concentrated purified DCLK1 variants (5 µg) were diluted to 400 µl in 100 mM
588 ammonium bicarbonate pH 8.0 (~40-fold dilution) prior to reduction (with dithiothreitol) and alkylation (with
589 iodoacetamide), as previously described by (69), and overnight digestion with a 25:1 (w/w) trypsin gold
590 (Promega) at 37 ^{o}C for 18 hours with 600 rpm shaking, Digests were then subject to strong cation
591 exchange using in-house packed stage tip clean-up (70). Dried peptides were solubilized in 20 µl of 3%
592 (v/v) acetonitrile and 0.1% (v/v) TFA in water, sonicated for 10 min, and centrifuged at 13,000 *g* for 10 min
593 at 4°C and supernatant collected. LC-MS/MS separation was performed using an Ultimate 3000 nano
594 system (Dionex), over a 60-min gradient (69). Briefly, samples were loaded at a rate of 12 µL/min onto a
595 trapping column (PepMap100, C18, 300 µm × 5 mm) in loading buffer (3% (v/v) acetonitrile, 0.1% (v/v)

596 TFA). Samples were then resolved on an analytical column (Easy-Spray C18 75 µm × 500 mm, 2 µm
597 bead diameter column) using a gradient of 97% A (0.1% (v/v) formic acid): 3% B (80% (v/v) acetonitrile,
598 0.1% (v/v) formic acid) to 80% B over 30 min at a flow rate of 300 nL/min. All data acquisition was
599 performed using a QExactive Orbitrap mass spectrometer (Thermo Scientific), with higher-energy C-trap
600 dissociation (HCD) fragmentation set at 30% normalized collision energy for 2+ to 4+ charge states using
601 a top 10 DDA mode. MS1 spectra were acquired at a 70K resolution (at 200 *m/z*) over a range of 300 to
602 2000 *m/z*, AGC target = 1e6, maximum injection time = 250 ms. MS2 spectra were acquired at a 17.5K
603 resolution (at 200 *m/z*), AGC target = 1e5, maximum injection time = 50 ms. A dynamic exclusion window
604 of 20 s was applied at a 10 ppm mass tolerance. Data was analysed by Proteome Discoverer 2.4 with the
605 MASCOT search engine using a custom database of the UniProt *Escherichia coli* reviewed database
606 (Updated January 2023) with the DCLK1 variants added, using the search parameters: fixed modification
607 = carbamidomethylation (C), variable modifications = oxidation (M) and phospho (S/T/Y), instrument type
608 = electrospray ionization–Fourier-transform ion cyclotron resonance (ESI-FTICR), MS1 mass tolerance =
609 10 ppm, MS2 mass tolerance = 0.01 Da, and the *ptm*RS node on; set to a score > 99.0. For label free
610 relative quantification of phosphopeptide abundances of the different DCLK1 variants, the minora feature
611 detector was active and set to calculate the area under the peak for peptide *m/z* ions. Phosphopeptide ion
612 abundances were normalized against 2 non-modified peptides to account for potential protein load
613 variability during analysis.
614
615 **DCLK1 DSF.** Thermal Shift Assays (TSA), were performed using Differential Scanning Fluorimetry (DSF)
616 in a StepOnePlus Real-Time PCR machine (Life Technologies) in combination with Sypro-Orange dye
617 (Invitrogen) and a thermal ramping protocol (0.3°C per minute between 25 and 94°C). Recombinant
618 DCLK1 proteins were assayed at a final concentration of 5 µM in 50 mM Tris–HCl (pH 7.4) and 100 mM
619 NaCl in the presence or absence of the indicated concentrations of ligand (ATP or Mg:ATP) or DCLK1
620 inhibitor compounds, with final DMSO concentrations never higher than 4% (v/v). Thermal melting data
621 were processed using the Boltzmann equation to generate sigmoidal denaturation curves, and
622 average $T_m/\Delta T_m$ values were calculated as described using GraphPad Prism software, as previously
623 described, from 3 technical repeats (71).
624
625 **DCLK1 kinase assays.** DCLK1 peptide-based enzyme assays were carried out using the LabChip EZ
626 Reader platform, which monitors and quantifies real-time phosphorylation-induced changes in the mobility
627 of the fluorescently labelled DCLK1 peptide substrate 5-FAM-KKALRRQETVDAL-$CONH_2$. To assess
628 DCLK1 catalytic domains, or DCLK1.1 or DCLK1.2 variants, 100ng of purified protein were incubated with
629 1 mM ATP (to mimic the cellular concentration) and 2 µM of the fluorescent substrate in 25 mM HEPES
630 (pH 7.4), 5 mM $MgCl_2$, and 0.001% (v/v) Brij 35. DCLK1-IN-1 -mediated enzyme inhibition was measured
631 under identical assay conditions in the presence of 10 µM of the inhibitor. Assays are either reported as
632 rates (pmoles/min phosphate incorporation) during linear phosphate incorporation (e.g total substrate

633 phosphorylation limited to <20-30% to prevent ATP depletion and to ensure assay linearity), or presented
634 as time-dependent percentage substrate phosphorylation (kinetic mode). All enzyme rate and kinetic data
635 are presented as mean and SD of 4 technical replicates.
636 **Author Contributions.** N.K. conceptualization; A.V., G.W., D.P.B., C.E.E., P.A.E., and N.K.
637 methodology; A.V., G.W., D.P.B., B.O., S.S., N.G., E.E.F., and L.A.D. investigation; A.V., G.W., and B.O.,
638 W.Y. data curation; A.V., G.W., D.P.B., B.O., and S.S. formal analysis; A.V., G.W., D.P.B.., and N.G.
639 validation; A.V., G.W., D.P.B., P.A.E., and N.K. writing – original draft; A.V., G.W., D.P.B., B.O., S.S.,
640 N.G., E.E.F., L.A.D., C.B., W.Y., I.A., S.K., C.E.E., P.A.E., and N.K. writing – review and editing; A.V.,
641 G.W., D.P.B., B.O., and S.S. visualization; P.A.E. and N.K. supervision; A.V., D.P.B., E.E.F., L.A.D.,
642 C.E.E., P.A.E., and N.K. funding acquisition.
643
644 **Funding and additional information.** Funding from N.K. (grant no.: R35 GM139656) is acknowledged.
645 P.A.E. acknowledges funding from the University of Liverpool BBSRC IAA award. A.V. acknowledges
646 funding from ARCS Foundation. D.P.B, L.A.D., P.A.E. and C.E.E. also acknowledge BBSRC grants
647 BB/S018514/1, BB/N021703/1 and BB/X002780/1 and North West Cancer Research (NWCR) grant
648 CR1208. E.E.F. thanks the MRC for a DiMeN DTP studentship (No. 1961582). The content is solely the
649 responsibility of the authors and does not necessarily represent the official views of the National Institutes
650 of Health.
651
652 **Data Availability.** All data generated in this study are included within the manuscript. Source data are
653 provided for each figure. MD simulations and associated data may be accessed from
654 https://www.dropbox.com/sh/xtiwpjgyzxy1oz0/AACK6dS3ypzYXDih3wgKp9bla?dl=0.
655
656 **Competing Interest Statement.** The authors claim no competing interest.
657

658 **References**

659 1. Manning G, Whyte DB, Martinez R, Hunter T, Sudarsanam S. The protein kinase complement of the
660 human genome. Science. 2002 Dec 6;298(5600):1912–34.

661 2. Agulto RL, Rogers MM, Tan TC, Ramkumar A, Downing AM, Bodin H, et al. Autoregulatory control of
662 microtubule binding in doublecortin-like kinase 1. Carter AP, Sengupta P, editors. eLife. 2021 Jul
663 26;10:e60126.

664 3. Bayer KU, Schulman H. CaM Kinase: Still Inspiring at 40. Neuron. 2019 Aug 7;103(3):380–94.

665 4. Gógl G, Kornev AP, Reményi A, Taylor SS. Disordered Protein Kinase Regions in Regulation of
666 Kinase Domain Cores. Trends Biochem Sci. 2019 Apr;44(4):300–11.

667 5. Berginski ME, Moret N, Liu C, Goldfarb D, Sorger PK, Gomez SM. The Dark Kinase Knowledgebase:
668 an online compendium of knowledge and experimental results of understudied kinases. Nucleic Acids
669 Res. 2021 Jan 8;49(D1):D529–35.

670 6. Sossey-Alaoui K, Srivastava AK. DCAMKL1, a brain-specific transmembrane protein on 13q12.3 that
671 is similar to doublecortin (DCX). Genomics. 1999 Feb 15;56(1):121–6.

672 7. Ohmae S, Takemoto-Kimura S, Okamura M, Adachi-Morishima A, Nonaka M, Fuse T, et al.
673 Molecular identification and characterization of a family of kinases with homology to
674 Ca2+/calmodulin-dependent protein kinases I/IV. J Biol Chem. 2006 Jul 21;281(29):20427–39.

675 8. Couillard-Despres S, Winner B, Schaubeck S, Aigner R, Vroemen M, Weidner N, et al. Doublecortin
676 expression levels in adult brain reflect neurogenesis. European Journal of Neuroscience.
677 2005;21(1):1–14.

678 9. Horesh D, Sapir T, Francis F, Grayer Wolf S, Caspi M, Elbaum M, et al. Doublecortin, a Stabilizer of
679 Microtubules. Human Molecular Genetics. 1999 Sep 1;8(9):1599–610.

680 10. Cheng L, Huang S, Chen L, Dong X, Zhang L, Wu C, et al. Research Progress of DCLK1 Inhibitors
681 as Cancer Therapeutics. Curr Med Chem. 2022;29(13):2261–73.

682 11. Gao T, Wang M, Xu L, Wen T, Liu J, An G. DCLK1 is up-regulated and associated with metastasis
683 and prognosis in colorectal cancer. J Cancer Res Clin Oncol. 2016 Oct 1;142(10):2131–40.

684 12. Westphalen CB, Quante M, Wang TC. Functional implication of Dclk1 and Dclk1-expressing cells in
685 cancer. Small GTPases. 2017 Jul 3;8(3):164–71.

686 13. Galvan L, Francelle L, Gaillard MC, de Longprez L, Carrillo-de Sauvage MA, Liot G, et al. The striatal
687 kinase DCLK3 produces neuroprotection against mutant huntingtin. Brain. 2018 May 1;141(5):1434–
688 54.

689 14. Kannan N, Haste N, Taylor SS, Neuwald AF. The hallmark of AGC kinase functional divergence is its
690 C-terminal tail, a cis-acting regulatory module. Proc Natl Acad Sci U S A. 2007 Jan 23;104(4):1272–
691 7.

692 15. Yeon JH, Heinkel F, Sung M, Na D, Gsponer J. Systems-wide Identification of cis-Regulatory
693 Elements in Proteins. Cell Syst. 2016 Feb 24;2(2):89–100.

694 16. Nguyen T, Ruan Z, Oruganty K, Kannan N. Co-conserved MAPK features couple D-domain docking
695 groove to distal allosteric sites via the C-terminal flanking tail. PLoS One. 2015;10(3):e0119636.

696 17. Yeung W, Kwon A, Taujale R, Bunn C, Venkat A, Kannan N. Evolution of Functional Diversity in the
697 Holozoan Tyrosine Kinome. Mol Biol Evol. 2021 Dec 9;38(12):5625–39.

698 18. Kwon A, John M, Ruan Z, Kannan N. Coupled regulation by the juxtamembrane and sterile α motif
699 (SAM) linker is a hallmark of ephrin tyrosine kinase evolution. J Biol Chem. 2018 Apr
700 6;293(14):5102–16.

701 19. Rellos P, Pike ACW, Niesen FH, Salah E, Lee WH, von Delft F, et al. Structure of the
702 CaMKIIdelta/calmodulin complex reveals the molecular mechanism of CaMKII kinase activation.
703 PLoS Biol. 2010 Jul 27;8(7):e1000426.

704 20. Bhattacharyya M, Lee YK, Muratcioglu S, Qiu B, Nyayapati P, Schulman H, et al. Flexible linkers in
705 CaMKII control the balance between activating and inhibitory autophosphorylation. Elife. 2020 Mar
706 9;9:e53670.

707 21. Hudmon A, Schulman H. Structure-function of the multifunctional Ca2+/calmodulin-dependent protein
708 kinase II. Biochem J. 2002 Jun 15;364(Pt 3):593–611.

709 22. Huse M, Kuriyan J. The conformational plasticity of protein kinases. Cell. 2002 May 3;109(3):275–82.

710 23. Wayman GA, Lee YS, Tokumitsu H, Silva AJ, Soderling TR. Calmodulin-kinases: modulators of
711 neuronal development and plasticity. Neuron. 2008 Sep 25;59(6):914–31.

712 24. Omori Y, Suzuki M, Ozaki K, Harada Y, Nakamura Y, Takahashi E, et al. Expression and
713 chromosomal localization of KIAA0369, a putative kinase structurally related to Doublecortin. J Hum
714 Genet. 1998;43(3):169–77.

715 25. Matsumoto N, Pilz DT, Ledbetter DH. Genomic structure, chromosomal mapping, and expression
716 pattern of human DCAMKL1 (KIAA0369), a homologue of DCX (XLIS). Genomics. 1999 Mar
717 1;56(2):179–83.

718 26. Cheng L, Yang Z, Guo W, Wu C, Liang S, Tong A, et al. DCLK1 autoinhibition and activation in
719 tumorigenesis. Innovation (Camb). 2022 Jan 25;3(1):100191.

720 27. Patel O, Roy MJ, Kropp A, Hardy JM, Dai W, Lucet IS. Structural basis for small molecule targeting of
721 Doublecortin Like Kinase 1 with DCLK1-IN-1. Commun Biol. 2021 Sep 20;4(1):1105.

722 28. Byrne DP, Shrestha S, Galler M, Cao M, Daly LA, Campbell AE, et al. Aurora A regulation by
723 reversible cysteine oxidation reveals evolutionarily conserved redox control of Ser/Thr protein kinase
724 activity. Sci Signal. 2020 Jul 7;13(639):eaax2713.

725 29. Ferguson FM, Nabet B, Raghavan S, Liu Y, Leggett AL, Kuljanin M, et al. Discovery of a selective
726 inhibitor of doublecortin like kinase 1. Nat Chem Biol. 2020 Jun;16(6):635–43.

727 30. Neuwald AF. A Bayesian Sampler for Optimization of Protein Domain Hierarchies. Journal of
728 Computational Biology. 2014 Feb 4;21(3):269–86.

729 31. Rosenberg OS, Deindl S, Sung RJ, Nairn AC, Kuriyan J. Structure of the autoinhibited kinase domain
730 of CaMKII and SAXS analysis of the holoenzyme. Cell. 2005 Dec 2;123(5):849–60.

731 32. Goldberg J, Nairn AC, Kuriyan J. Structural basis for the autoinhibition of calcium/calmodulin-
732 dependent protein kinase I. Cell. 1996 Mar 22;84(6):875–87.

733 33. Zheng J, Trafny EA, Knighton DR, Xuong NH, Taylor SS, Ten Eyck LF, et al. 2.2 A refined crystal
734 structure of the catalytic subunit of cAMP-dependent protein kinase complexed with MnATP and a
735 peptide inhibitor. Acta Crystallogr D Biol Crystallogr. 1993 May 1;49(Pt 3):362–5.

736 34. Romano RA, Kannan N, Kornev AP, Allison CJ, Taylor SS. A chimeric mechanism for polyvalent
737 trans-phosphorylation of PKA by PDK1. Protein Science. 2009;18(7):1486–97.

738 35. Baffi TR, Newton AC. mTOR Regulation of AGC Kinases: New Twist to an Old Tail. Mol Pharmacol.
739 2022 Apr 1;101(4):213–8.

740 36. Taylor SS, Kornev AP. Protein kinases: evolution of dynamic regulatory proteins. Trends Biochem
741 Sci. 2011 Feb;36(2):65–77.

742 37. Yokokura H, Picciotto MR, Nairn AC, Hidaka H. The regulatory region of calcium/calmodulin-
743 dependent protein kinase I contains closely associated autoinhibitory and calmodulin-binding
744 domains. J Biol Chem. 1995 Oct 6;270(40):23851–9.

745 38. Yang E, Schulman H. Structural examination of autoregulation of multifunctional calcium/calmodulin-
746 dependent protein kinase II. J Biol Chem. 1999 Sep 10;274(37):26199–208.

747 39. Eyers PA. TRIBBLES: A Twist in the Pseudokinase Tail. Structure. 2015 Nov 3;23(11):1974–6.

748 40. Eyers PA, Keeshan K, Kannan N. Tribbles in the 21st Century: The Evolving Roles of Tribbles
749 Pseudokinases in Biology and Disease. Trends Cell Biol. 2017 Apr;27(4):284–98.

750 41. Foulkes DM, Byrne DP, Yeung W, Shrestha S, Bailey FP, Ferries S, et al. Covalent inhibitors of
751 EGFR family protein kinases induce degradation of human Tribbles 2 (TRIB2) pseudokinase in
752 cancer cells. Sci Signal. 2018 Sep 25;11(549):eaat7951.

753 42. Harris JA, Fairweather E, Byrne DP, Eyers PA. Analysis of human Tribbles 2 (TRIB2) pseudokinase.
754 Methods Enzymol. 2022;667:79–99.

755 43. Keeshan K, Bailis W, Dedhia PH, Vega ME, Shestova O, Xu L, et al. Transformation by Tribbles
756 homolog 2 (Trib2) requires both the Trib2 kinase domain and COP1 binding. Blood. 2010 Dec
757 2;116(23):4948–57.

758 44. Murphy JM, Nakatani Y, Jamieson SA, Dai W, Lucet IS, Mace PD. Molecular Mechanism of CCAAT-
759 Enhancer Binding Protein Recruitment by the TRIB1 Pseudokinase. Structure. 2015 Nov
760 3;23(11):2111–21.

761 45. Burgess HA, Reiner O. Alternative splice variants of doublecortin-like kinase are differentially
762 expressed and have different kinase activities. J Biol Chem. 2002 May 17;277(20):17696–705.

763 46. Qu D, Weygant N, Yao J, Chandrakesan P, Berry WL, May R, et al. Overexpression of DCLK1-AL
764 Increases Tumor Cell Invasion, Drug Resistance, and KRAS Activation and Can Be Targeted to
765 Inhibit Tumorigenesis in Pancreatic Cancer. J Oncol. 2019;2019:6402925.

766 47. Ding L, Yang Y, Ge Y, Lu Q, Yan Z, Chen X, et al. Inhibition of DCLK1 with DCLK1-IN-1 Suppresses
767 Renal Cell Carcinoma Invasion and Stemness and Promotes Cytotoxic T-Cell-Mediated Anti-Tumor
768 Immunity. Cancers (Basel). 2021 Nov 16;13(22):5729.

769 48. Major J, Szende B, Lapis K, Thész Z. Increased SCE inducibility by low doses of methylcholanthrene
770 in lymphocytes obtained from patients with Down's disease. Mutat Res. 1985 Mar;149(1):51–5.

771 49. Huang LC, Taujale R, Gravel N, Venkat A, Yeung W, Byrne DP, et al. KinOrtho: a method for
772 mapping human kinase orthologs across the tree of life and illuminating understudied kinases. BMC
773 Bioinformatics. 2021 Sep 18;22(1):446.

774 50. UniProt Consortium. UniProt: the universal protein knowledgebase in 2021. Nucleic Acids Res. 2021
775 Jan 8;49(D1):D480–9.

776 51. Neuwald AF. Rapid detection, classification and accurate alignment of up to a million or more related
777 protein sequences. Bioinformatics. 2009 Aug 1;25(15):1869–75.

778 52. Nguyen LT, Schmidt HA, von Haeseler A, Minh BQ. IQ-TREE: a fast and effective stochastic
779 algorithm for estimating maximum-likelihood phylogenies. Mol Biol Evol. 2015 Jan;32(1):268–74.

780 53. Hoang DT, Chernomor O, von Haeseler A, Minh BQ, Vinh LS. UFBoot2: Improving the Ultrafast
781 Bootstrap Approximation. Mol Biol Evol. 2018 Feb 1;35(2):518–22.

782 54. Le SQ, Gascuel O. An improved general amino acid replacement matrix. Mol Biol Evol. 2008
783 Jul;25(7):1307–20.

784 55. Gu X, Fu YX, Li WH. Maximum likelihood estimation of the heterogeneity of substitution rate among
785 nucleotide sites. Mol Biol Evol. 1995 Jul;12(4):546–57.

786 56. Kalyaanamoorthy S, Minh BQ, Wong TKF, von Haeseler A, Jermiin LS. ModelFinder: fast model
787 selection for accurate phylogenetic estimates. Nat Methods. 2017 Jun;14(6):587–9.

788 57. Huerta-Cepas J, Serra F, Bork P. ETE 3: Reconstruction, Analysis, and Visualization of
789 Phylogenomic Data. Mol Biol Evol. 2016 Jun;33(6):1635–8.

790 58. Katoh K, Misawa K, Kuma K ichi, Miyata T. MAFFT: a novel method for rapid multiple sequence
791 alignment based on fast Fourier transform. Nucleic Acids Res. 2002 Jul 15;30(14):3059–66.

792 59. Mandell DJ, Coutsias EA, Kortemme T. Sub-angstrom accuracy in protein loop reconstruction by
793 robotics-inspired conformational sampling. Nat Methods. 2009 Aug;6(8):551–2.

794 60. Tyka MD, Keedy DA, André I, Dimaio F, Song Y, Richardson DC, et al. Alternate states of proteins
795 revealed by detailed energy landscape mapping. J Mol Biol. 2011 Jan 14;405(2):607–18.

796 61. Michaud-Agrawal N, Denning EJ, Woolf TB, Beckstein O. MDAnalysis: a toolkit for the analysis of
797 molecular dynamics simulations. J Comput Chem. 2011 Jul 30;32(10):2319–27.

798 62. Jorgensen WL, Chandrasekhar J, Madura JD, Impey RW, Klein ML. Comparison of simple potential
799 functions for simulating liquid water. J Chem Phys. 1983 Jul 15;79(2):926–35.

800 63. Pronk S, Páll S, Schulz R, Larsson P, Bjelkmar P, Apostolov R, et al. GROMACS 4.5: a high-
801 throughput and highly parallel open source molecular simulation toolkit. Bioinformatics. 2013 Apr
802 1;29(7):845–54.

803 64. Huang J, MacKerell AD. CHARMM36 all-atom additive protein force field: validation based on
804 comparison to NMR data. J Comput Chem. 2013 Sep 30;34(25):2135–45.

805 65. Humphrey W, Dalke A, Schulten K. VMD: visual molecular dynamics. J Mol Graph. 1996
806 Feb;14(1):33–8, 27–8.

807 66. Park H, Bradley P, Greisen P, Liu Y, Mulligan VK, Kim DE, et al. Simultaneous Optimization of
808 Biomolecular Energy Functions on Features from Small Molecules and Macromolecules. J Chem
809 Theory Comput. 2016 Dec 13;12(12):6201–12.

810 67. Keller O, Odronitz F, Stanke M, Kollmar M, Waack S. Scipio: using protein sequences to determine
811 the precise exon/intron structures of genes and their orthologs in closely related species. BMC
812 Bioinformatics. 2008 Jun 13;9:278.

813 68. Cunningham F, Allen JE, Allen J, Alvarez-Jarreta J, Amode MR, Armean IM, et al. Ensembl 2022.
814 Nucleic Acids Res. 2022 Jan 7;50(D1):D988–95.

815 69. Ferries S, Perkins S, Brownridge PJ, Campbell A, Eyers PA, Jones AR, et al. Evaluation of
816 Parameters for Confident Phosphorylation Site Localization Using an Orbitrap Fusion Tribrid Mass
817 Spectrometer. J Proteome Res. 2017 Sep 1;16(9):3448–59.

818 70. Daly LA, Brownridge PJ, Batie M, Rocha S, Sée V, Eyers CE. Oxygen-dependent changes in binding
819 partners and post-translational modifications regulate the abundance and activity of HIF-1α/2α. Sci
820 Signal. 2021 Jul 20;14(692):eabf6685.

821 71. Byrne DP, Clarke CJ, Brownridge PJ, Kalyuzhnyy A, Perkins S, Campbell A, et al. Use of the Polo-
822 like kinase 4 (PLK4) inhibitor centrinone to investigate intracellular signalling networks using SILAC-
823 based phosphoproteomics. Biochem J. 2020 Jul 17;477(13):2451–75.

824

825 **Figure supplements for:**

826 # Mechanistic and evolutionary insights into isoform-specific 'supercharging' in
827 # DCLK family kinases

828

829 Aarya Venkat[1+], Grace Watterson[1+], Dominic P. Byrne[2+], Brady O'Boyle[1], Safal Shrestha[3], Nathan Gravel[3], Emma
830 E. Fairweather[2], Leonard A. Daly[2,4], Claire Bunn[1], Wayland Yeung[3], Ishan Aggarwal[1], Samiksha Katiyar[1], Claire E.
831 Eyers[2,4], Patrick A. Eyers[2*], and Natarajan Kannan[1,3*]

832

833 **Affiliations:**

834 [1]Department of Biochemistry and Molecular Biology, University of Georgia, Athens, GA 30602, USA
835 [2]Department of Biochemistry and Systems Biology, Institute of Systems, Molecular and Integrative Biology,
836 University of Liverpool, Liverpool, L69 7ZB, UK
837 [3]Institute of Bioinformatics, University of Georgia, Athens, GA 30602, USA
838 [4]Centre for Proteome Research, Department of Biochemistry and Systems Biology, Institute of Systems, Molecular
839 and Integrative Biology, University of Liverpool, Liverpool, L69 7ZB, UK
840
841 + equal contributions
842
843 *Correspondence to: Natarajan Kannan, Email: nkannan@uga.edu or Patrick Eyers, Email:
844 patrick.eyers@liverpool.ac.uk
845

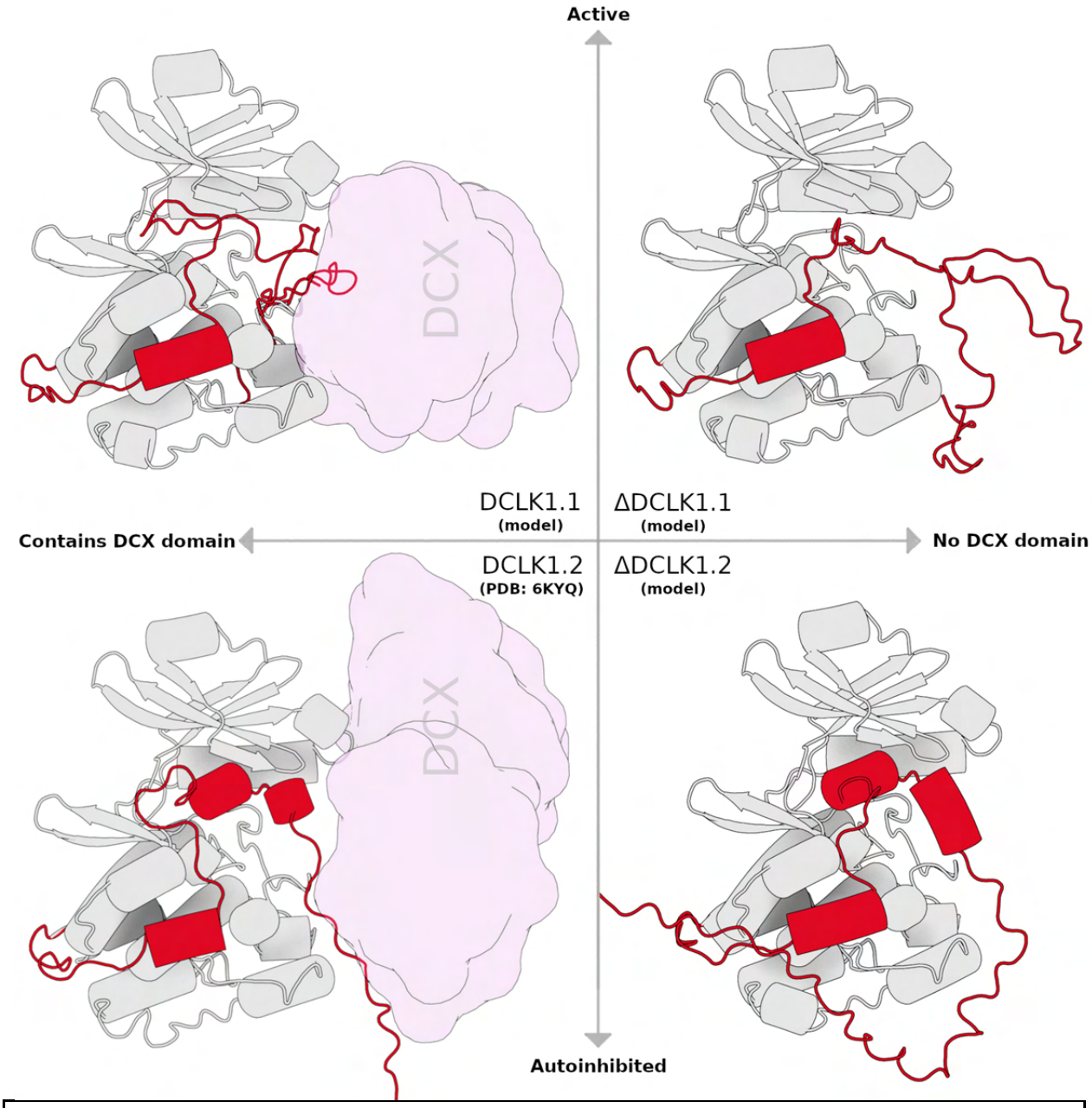

Figure 1-figure supplement 1: Structural cartoon depicting each DCLK1 isoform, categorizing them by presence of DCX domain and enzymatic activity.

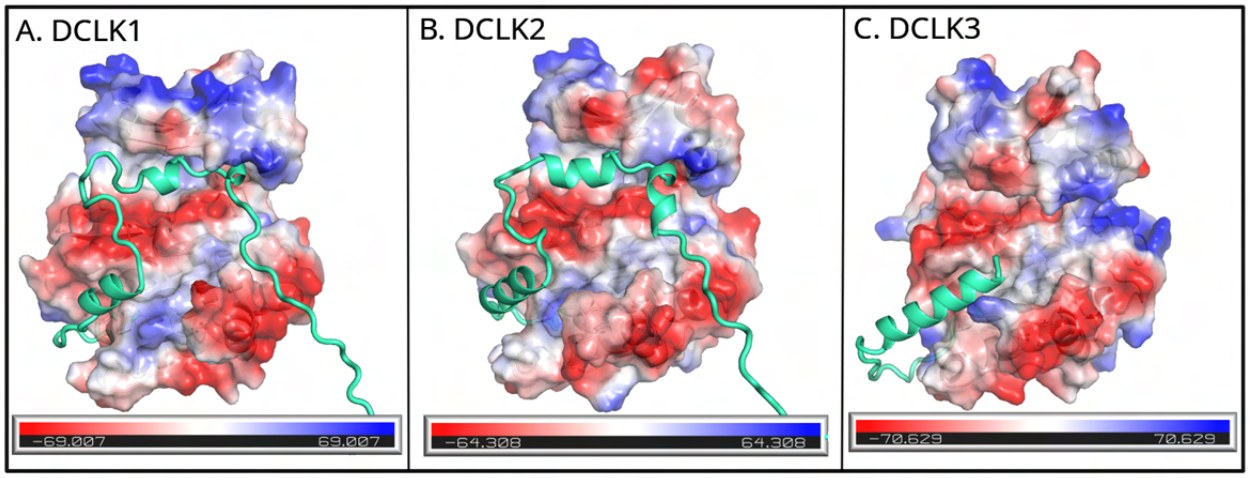

Figure 2-figure supplement 1: Each of the full-length DCLK paralogs showing how the tail packs against the substrate binding pocket of the kinase domain.

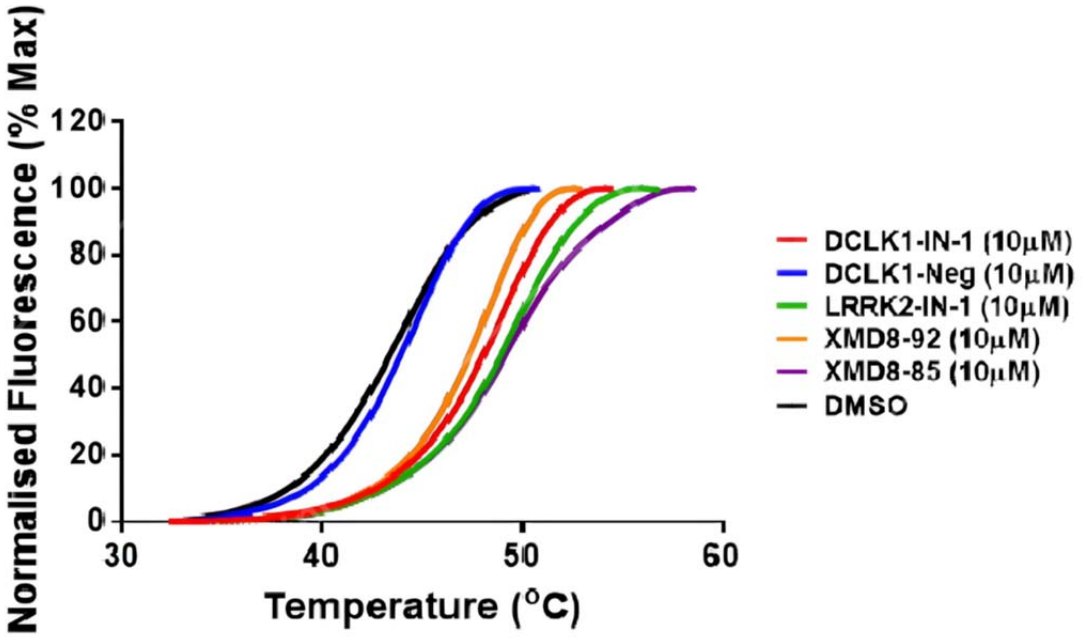

852

Figure 3-figure supplement 1: Fluorescence for $DCLK1_{cat}$ in presence of DMSO and different inhibitor conditions.

853
854

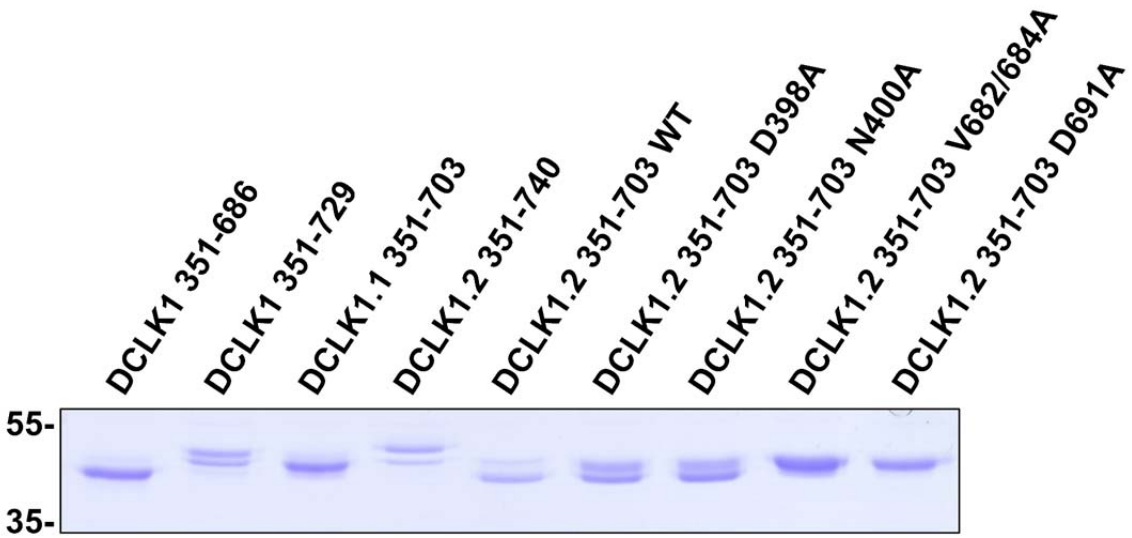

855
856

Figure 5-figure supplement 1: SDS-Page and Coomassie blue staining of each DCLK1 construct.

857

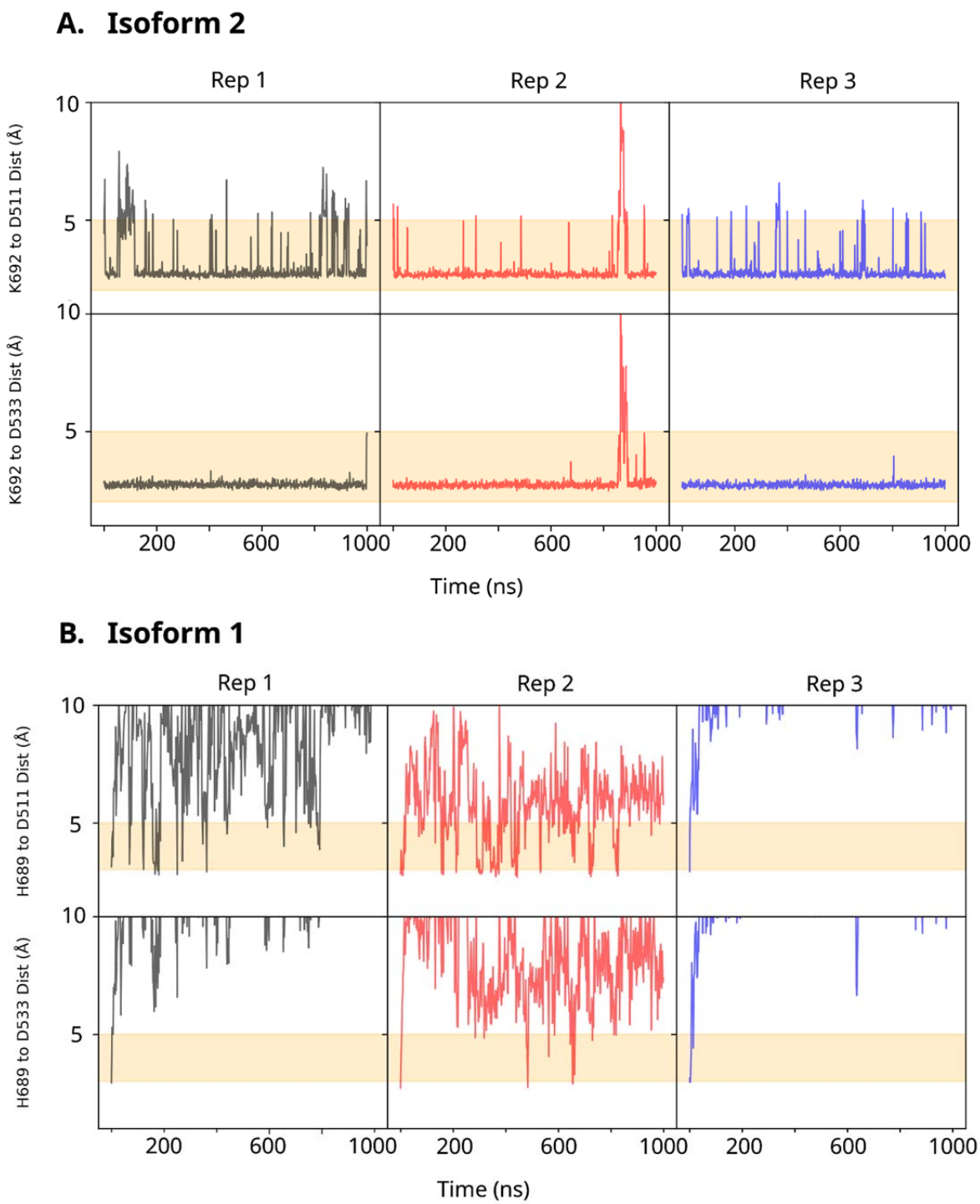

858

Figure 5-figure supplement 2: A) Minimum Distance of K692 in the DCLK1.2 C-tail forms significant stable interactions over microsecond replicates to the DFG and HRD aspartates. **B)** H689 in the DCLK1.1 C-tail, comparatively fails to interact with the DFG and HRD aspartates.

859

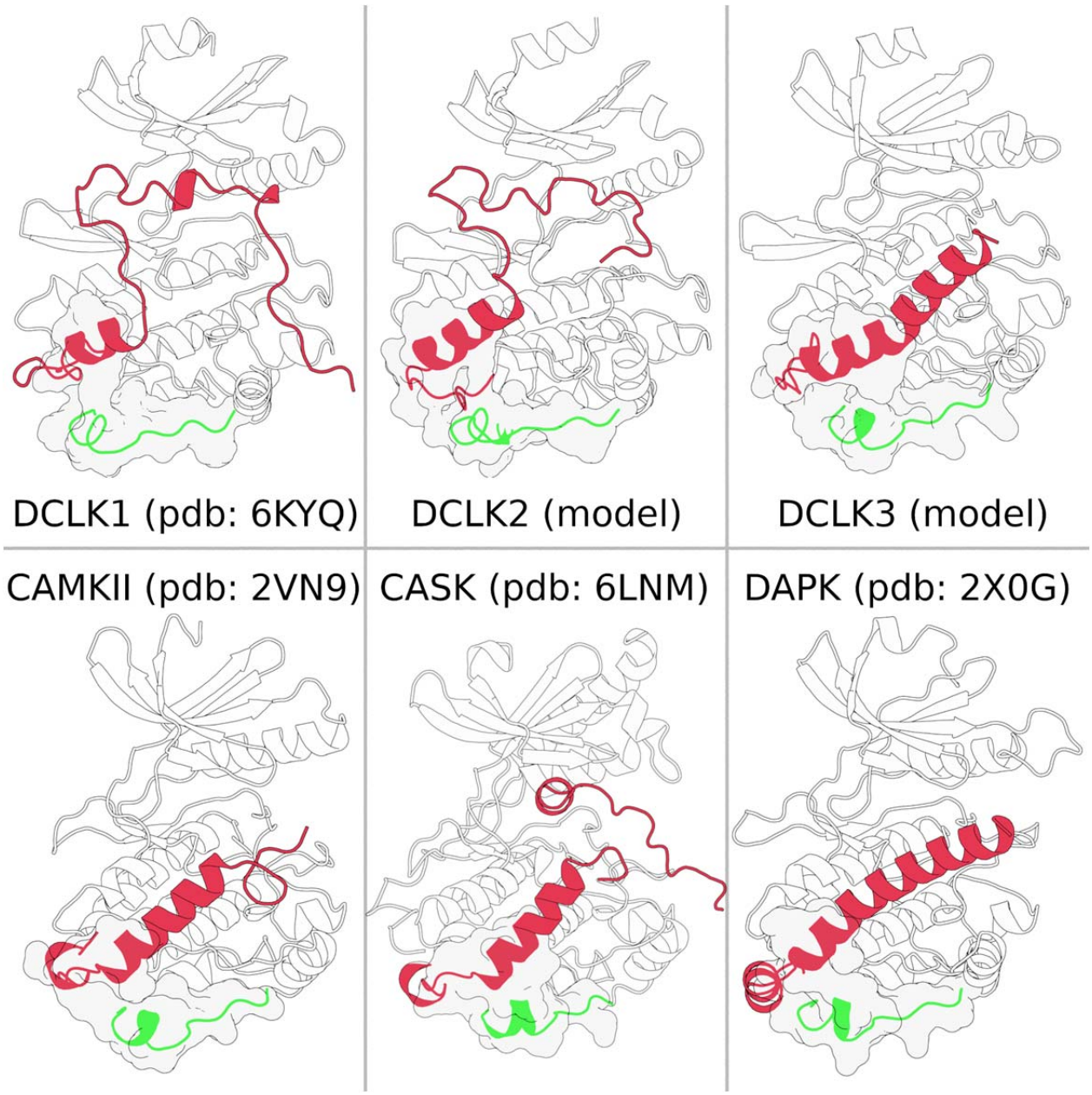

Figure 6-figure supplement 1: CAMK-specific insert (green) consistently making structural contacts (shown in surface representation) with the C-tail (red) across multiple CAMK families.

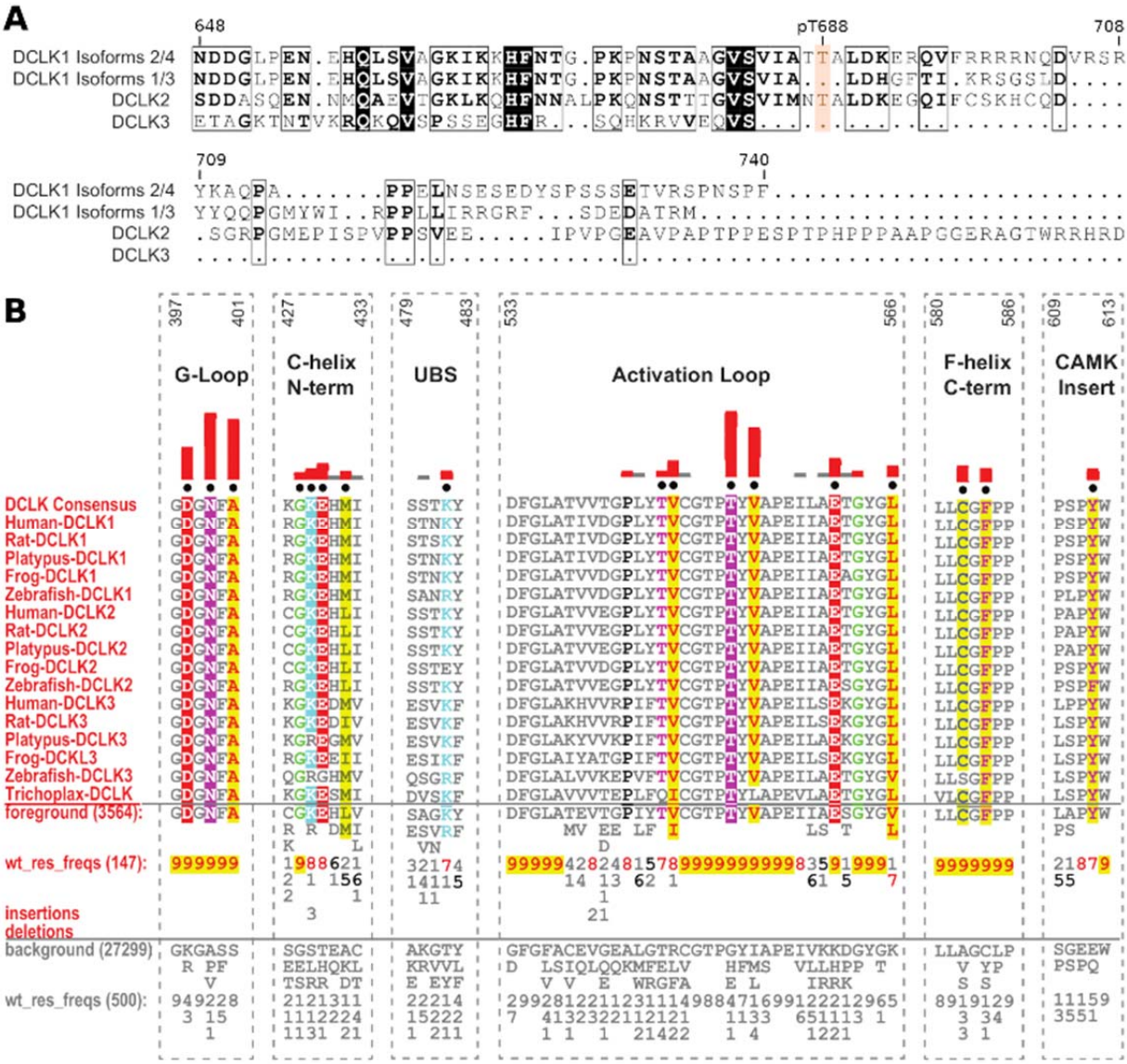

Figure 6-figure supplement 2: Identification of DCLK family-specific constraints. A) Sequence alignment of human DCLK paralogs including long and short isoforms of DCLK1. **B)** Sequence constraints that distinguish DCLK1/2/3 sequences from closely related CAMK sequences are shown in a contrast hierarchical alignment (CHA). The CHA shows DCLK1/2/3 sequences from diverse organisms as the display alignment. The foreground consists of 3564 DCLK sequences while the background alignment contains 27,299 related CAMK sequences. The foreground and background alignments are shown as residue frequencies below the display alignment in integer tenths (1–9). The histogram (red) indicates the extent to which distinguishing residues in the foreground diverge from the corresponding position in the background alignment. Black dots indicate the alignment positions used by the BPPS (Neuwald, 2014) procedure when classifying DCLK sequences from related CAMK sequences. Alignment number is based on the human DCLK1 sequence (Uniprot ID: O15075-1).

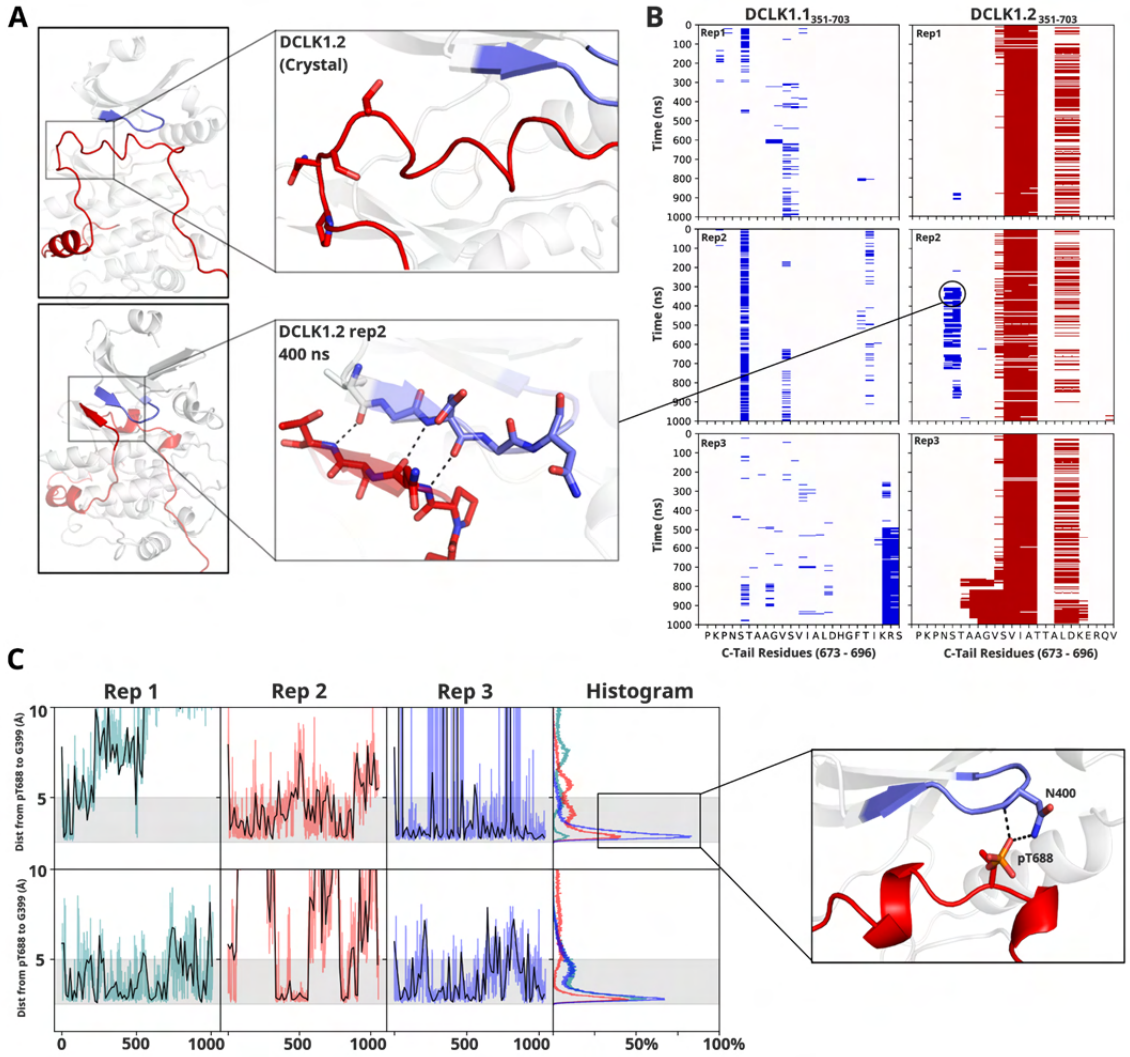

Figure 7-figure supplement 1: Molecular Dynamics of DCLK1 isoforms. **A-B)** Microsecond MD replicates from DCLK1.1 and DCLK1.2, showing the DSSP output plotted for the C-tail, where red lines represent alpha helices and blue lines represent beta sheets. **C)** Distance plots from MD replicates of the phosphorylated threonine highlighting the contact distance between pT688 phosphate and G399 of the G-loop.

A

Sequence	Phosphosite in protein (ptmRS score)	MASCOT score	DCLK1.1 (351-703)	DLCK1.2 (351-703)
GKEHMIQNEVSILR	Ser 438 (100)	68	1.00	0.15
FSAVQVLEHPWVNDDGLPENEHQLSVAGK	Ser 660 (100)	42	1.00	0.01

B

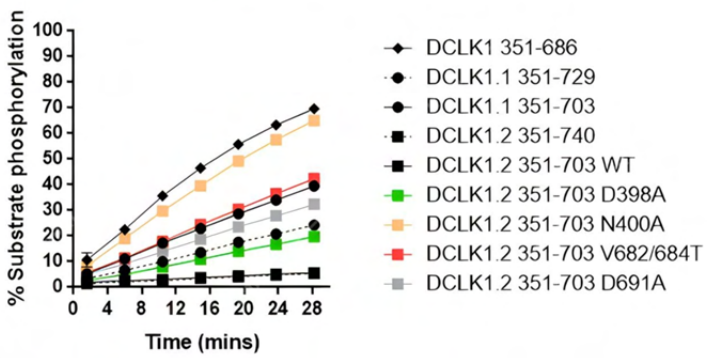

C

			Normalised fold change			
Sequence	Phosphosite in protein (ptmRS score)	MASCOT score	WT	D398A	N400A	V682/684T
TIGDGNFAVVK	Thr 395 (100)	60	1.00	ND	ND	1.41
GKEHMIQNEVSILR	Ser 438 (100)	69	1.00	6.91	4.08	1.69
DASGMLYNLASAIK	Ser 489 (100)	75	1.00	1.24	0.42	0.07
FSAVQVLEHPWVNDDGLPENEHQLSVAGK	Ser 660 (100)	50	1.00	99.01	41.43	43.76

Figure 8-figure supplement 1: A) Quantitative LC-MS/MS data showing tryptic phosphopeptides identified from DCLK1.1 and 1.2. Detailed are peptide sequences, identified sites of phosphorylation (red), the site of phosphorylation within the protein and the ptmRS score relevant to confidence of phosphosite localisation, as well as the Mascot score for peptide identification. Fold change in the relative abundance of the two phosphopeptides in DCLK 1.2 is computed with reference to these same two phosphopeptides in DCLK1.1., normalising against 3 non-modified peptides to account for potential difference in the amount analysed. **B**) DCLK1 substrate phosphorylation (reported as % total phosphopeptide in reaction) was quantified as a function of time for each of the indicated purified DCLK proteins. Assays were performed side-by-side in quadriplicate. **C)** As described in A, except fold change in abundance could not be calculated for the peptide containing pThr 395 given the presence of the inserted mutations and the potential differences in relative ionisation efficiency for the resulting tryptic peptide.

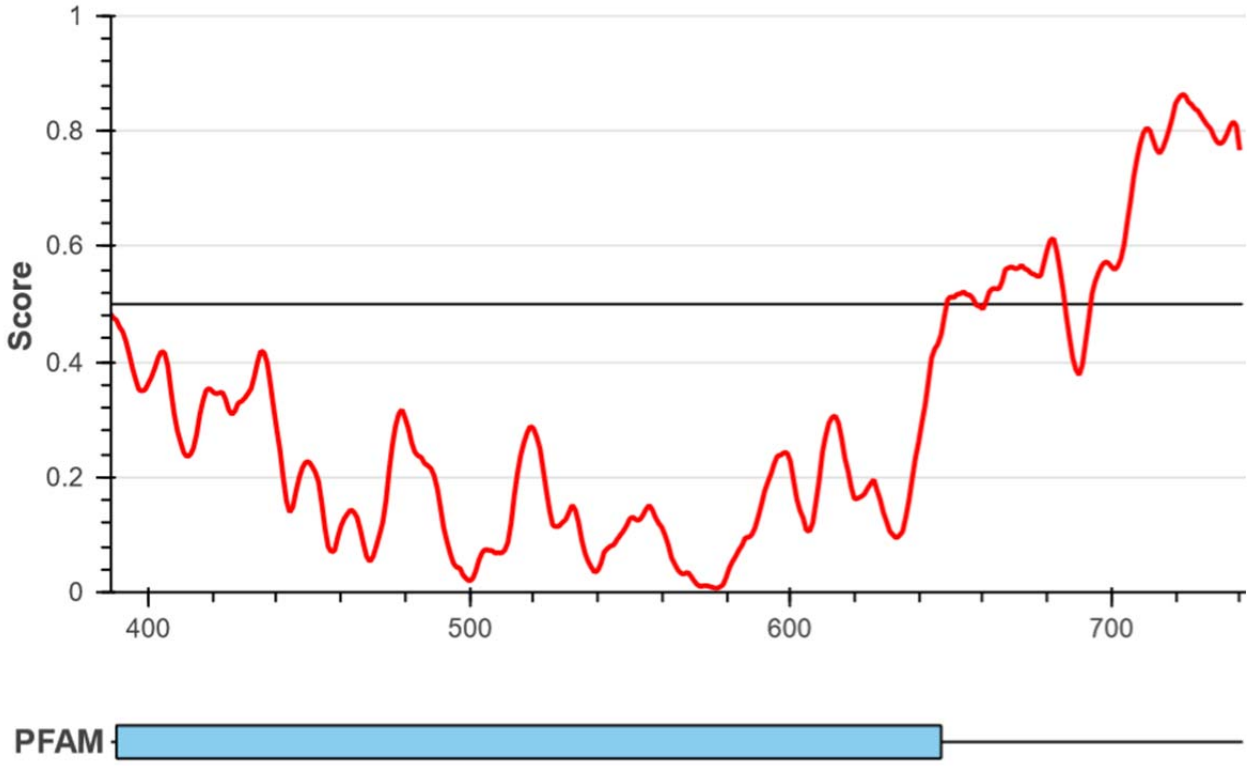

Figure 9-figure supplement 1: Intrinsic Disorder prediction of DCLK1.2 C-tail using IUPRED3.

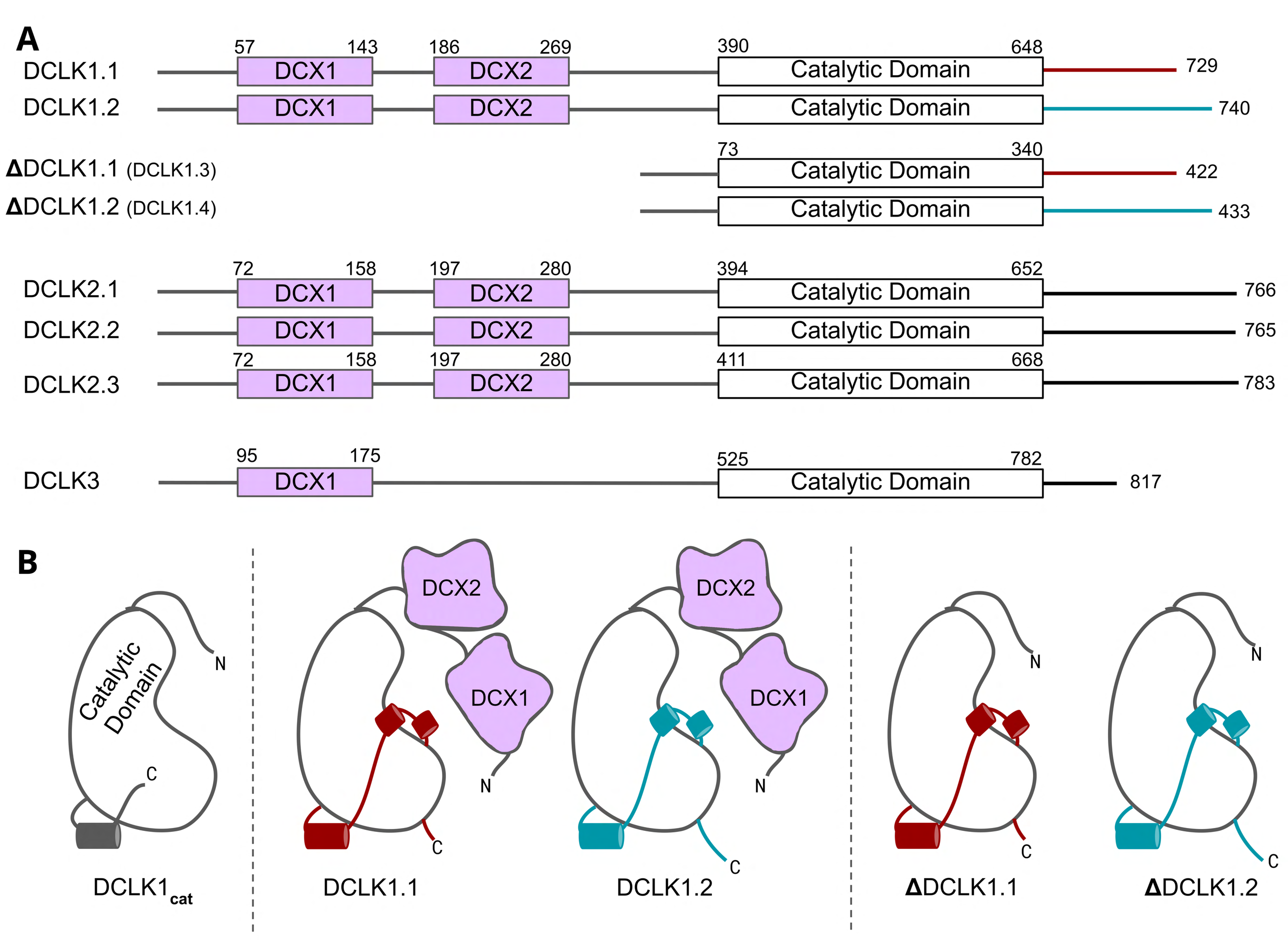
A
DCLK1.1
57
143
186
269
390
648
729
DCX1
DCX2
Catalytic Domain
DCLK1.2
740
ΔDCLK1.1 (DCLK1.3)
73
340
422
ΔDCLK1.2 (DCLK1.4)
433
DCLK2.1
72
158
197
280
394
652
766
DCLK2.2
765
DCLK2.3
411
668
783
DCLK3
95
175
525
782
817
B
Catalytic Domain
N
C
DCX2
DCX1
DCLK1cat
DCLK1.1
DCLK1.2
ΔDCLK1.1
ΔDCLK1.2

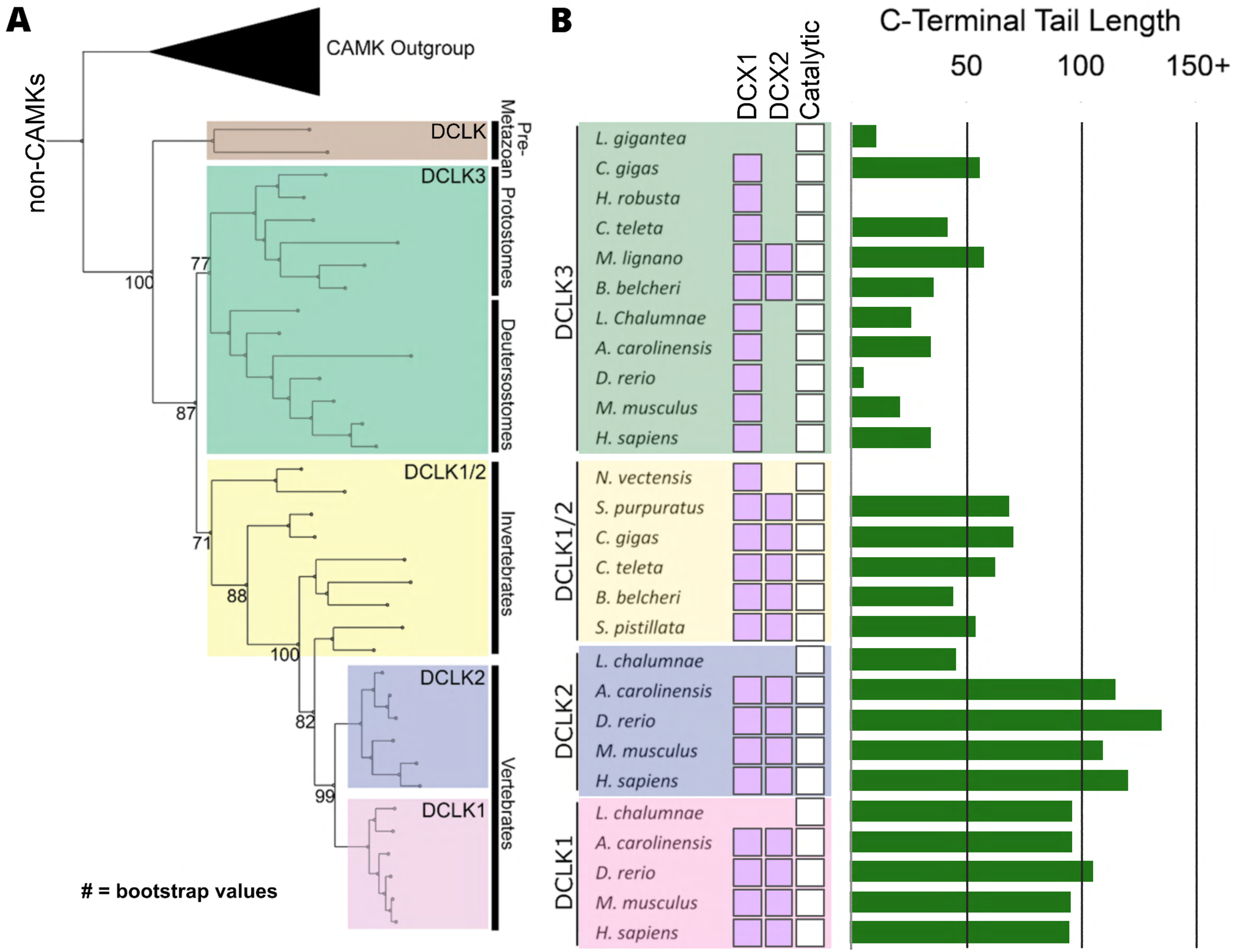
A
CAMK Outgroup
non-CAMKs
DCLK
DCLK3
DCLK1/2
DCLK2
DCLK1
Pre-Metazoan
Protostomes
Deutersostomes
Invertebrates
Vertebrates
100
77
87
71
88
100
82
99
= bootstrap values
B
C-Terminal Tail Length
50
100
150+
DCX1
DCX2
Catalytic
DCLK3
L. gigantea
C. gigas
H. robusta
C. teleta
M. lignano
B. belcheri
L. Chalumnae
A. carolinensis
D. rerio
M. musculus
H. sapiens
DCLK1/2
N. vectensis
S. purpuratus
C. gigas
C. teleta
B. belcheri
S. pistillata
DCLK2
L. chalumnae
A. carolinensis
D. rerio
M. musculus
H. sapiens
DCLK1
L. chalumnae
A. carolinensis
D. rerio
M. musculus
H. sapiens

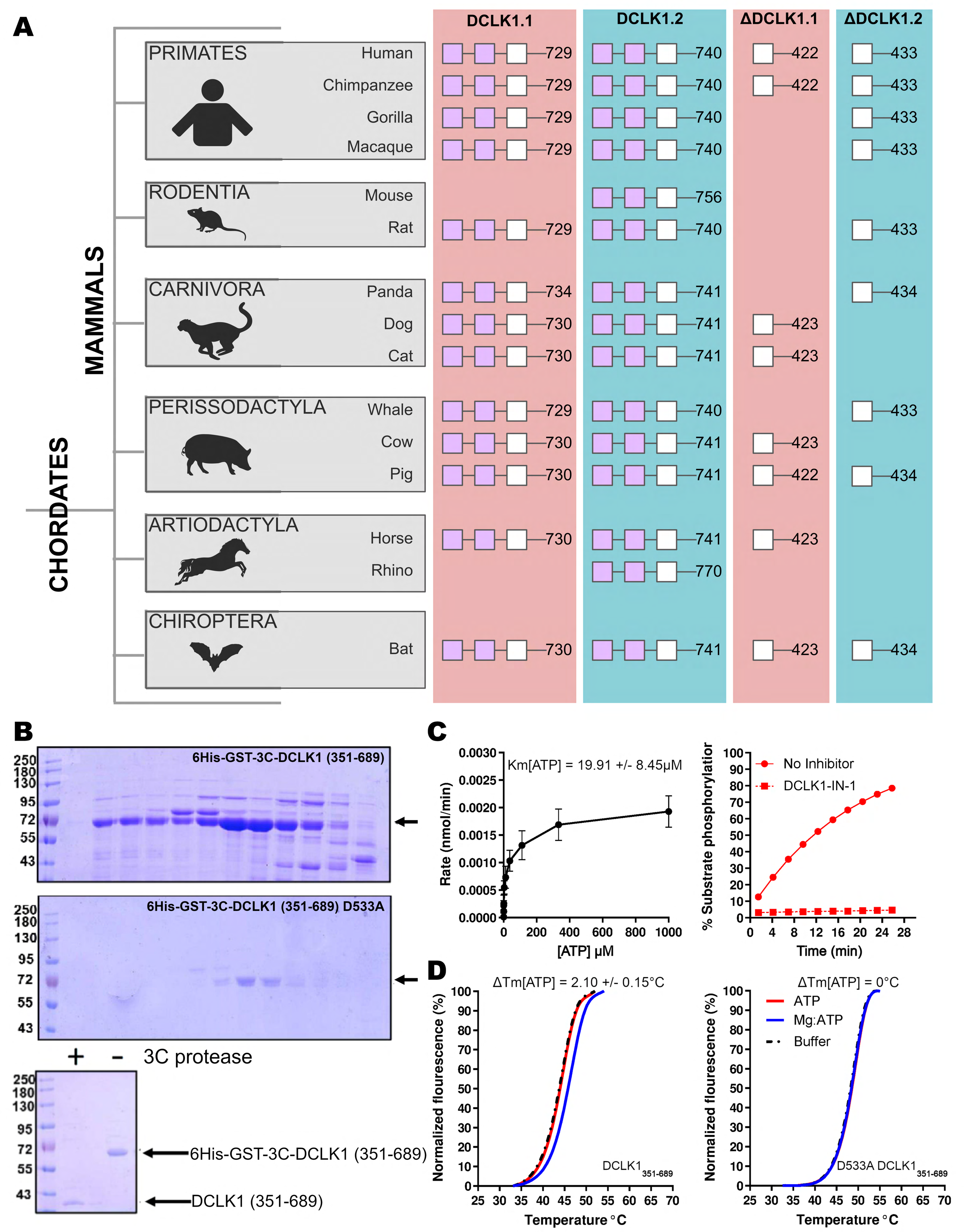
A
DCLK1.1
DCLK1.2
ΔDCLK1.1
ΔDCLK1.2
CHORDATES
MAMMALS
PRIMATES
Human
Chimpanzee
Gorilla
Macaque
RODENTIA
Mouse
Rat
CARNIVORA
Panda
Dog
Cat
PERISSODACTYLA
Whale
Cow
Pig
ARTIODACTYLA
Horse
Rhino
CHIROPTERA
Bat
B
6His-GST-3C-DCLK1 (351-689)
6His-GST-3C-DCLK1 (351-689) D533A
+ − 3C protease
6His-GST-3C-DCLK1 (351-689)
DCLK1 (351-689)
C
Km[ATP] = 19.91 +/- 8.45μM
Rate (nmol/min)
[ATP] μM
% Substrate phosphorylation
Time (min)
No Inhibitor
DCLK1-IN-1
D
ΔTm[ATP] = 2.10 +/- 0.15°C
ΔTm[ATP] = 0°C
ATP
Mg:ATP
Buffer
Normalized flourescence (%)
Temperature °C
DCLK1 351-689
D533A DCLK1 351-689

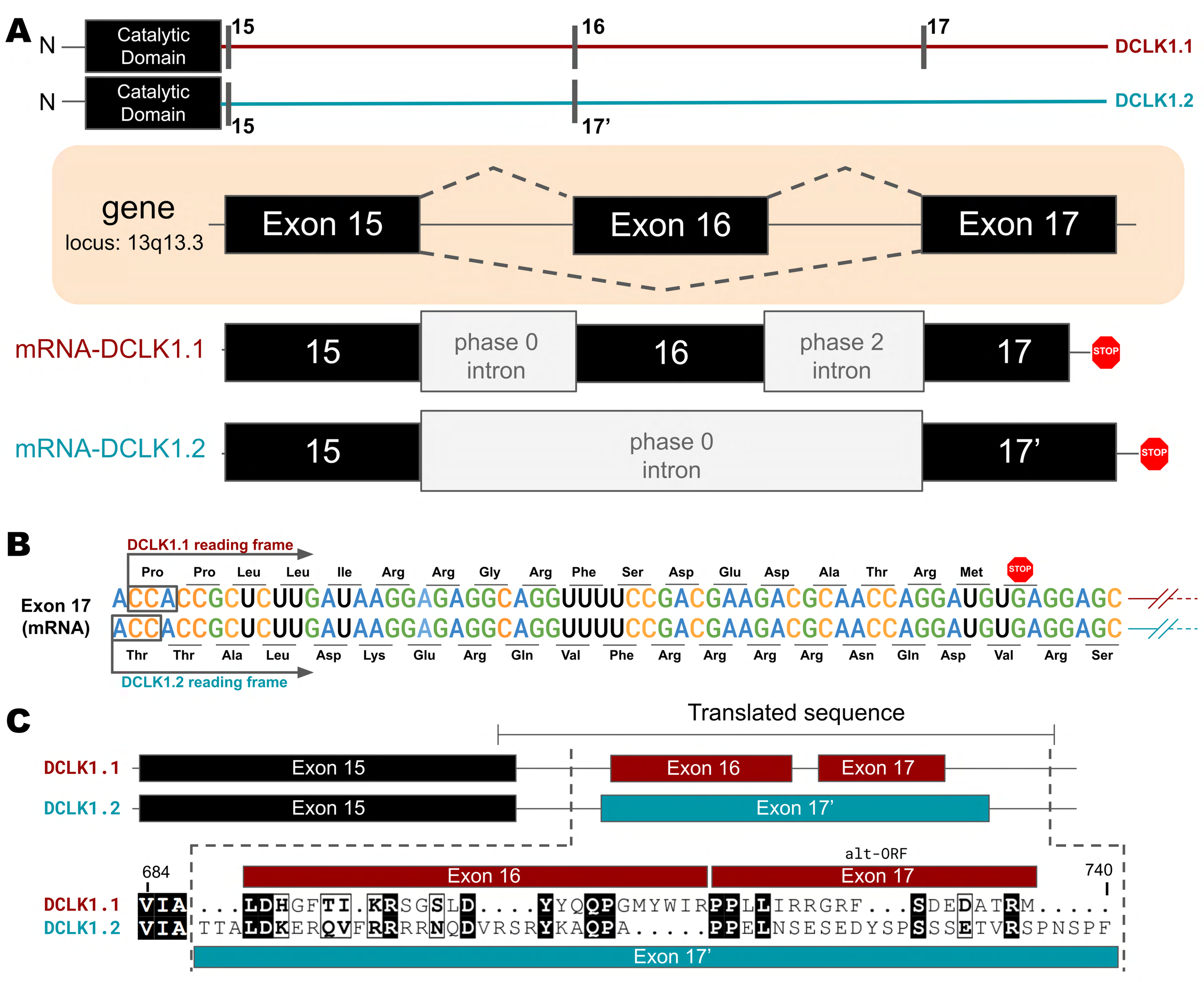
A
N
Catalytic Domain
15
16
17
DCLK1.1
N
Catalytic Domain
15
17'
DCLK1.2
gene
locus: 13q13.3
Exon 15
Exon 16
Exon 17
mRNA-DCLK1.1
15
phase 0 intron
16
phase 2 intron
17
STOP
mRNA-DCLK1.2
15
phase 0 intron
17'
STOP
B
DCLK1.1 reading frame
Pro Pro Leu Leu Ile Arg Arg Gly Arg Phe Ser Asp Glu Asp Ala Thr Arg Met STOP
Exon 17 (mRNA)
ACCACCGCUCUUGAUAAGGAGAGGCAGGUUUUCCGACGAAGACGCAACCAGGAUGUGAGGAGC
ACCACCGCUCUUGAUAAGGAGAGGCAGGUUUUCCGACGAAGACGCAACCAGGAUGUGAGGAGC
Thr Thr Ala Leu Asp Lys Glu Arg Gln Val Phe Arg Arg Arg Arg Asn Gln Asp Val Arg Ser
DCLK1.2 reading frame
C
Translated sequence
DCLK1.1
Exon 15
Exon 16
Exon 17
DCLK1.2
Exon 15
Exon 17'
alt-ORF
684
Exon 16
Exon 17
740
DCLK1.1 VIA ...LDHGFTI.KRSGSLD....YYQQPGMYWIRPPLLIRRGRF...SDEDATRM.....
DCLK1.2 VIA TTALDKERQVFRRRRNQDVRSRYKAQPA.....PPELNSESEDYSPSSSETVRSPNSPF
Exon 17'

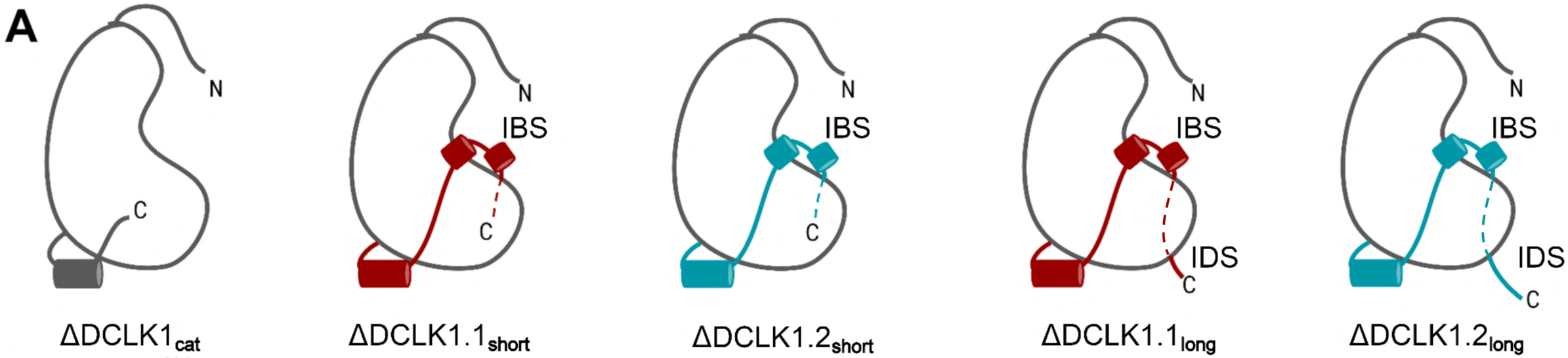

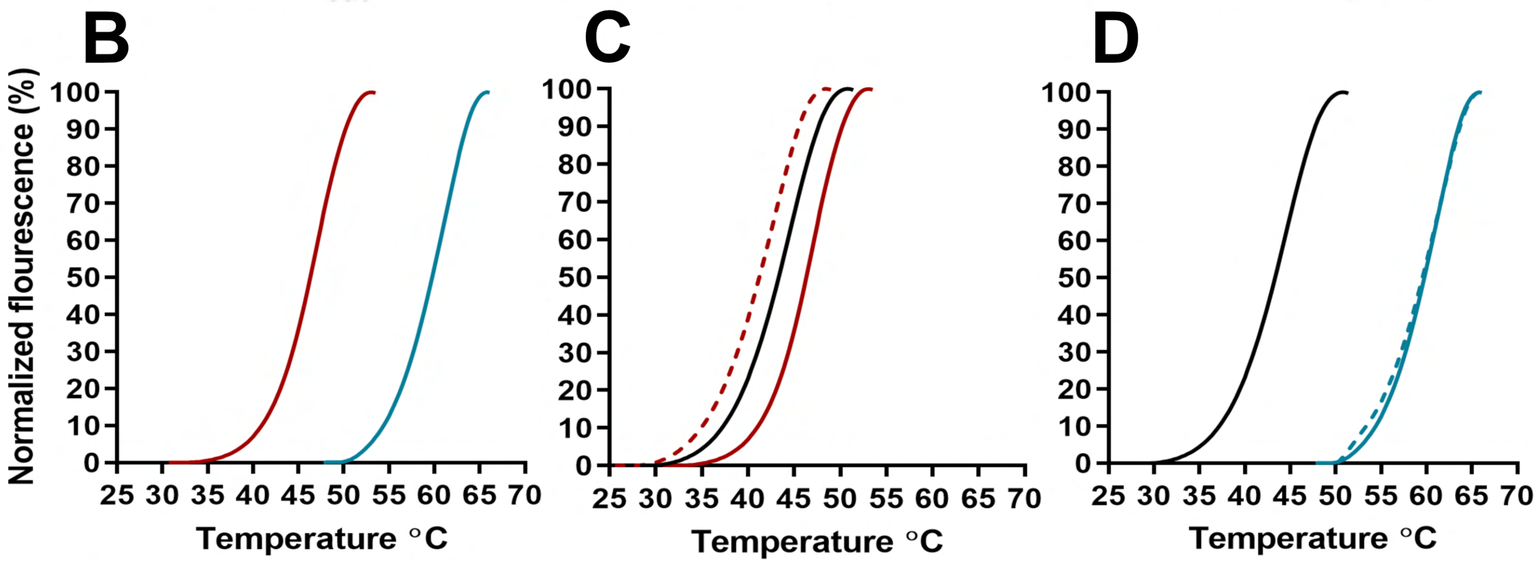

E

	Residues	Tm (°C)	ΔTm (°C)
DCLK1cat	351-686	43.7 ± 0.3	–
DCLK1.1short	351-703	46.8 ± 0.1	3.1
DCLK1.1long	351-729	41.8 ± 0.0	-1.9
DCLK1.2short	351-703	60.2 ± 0.1	16.5
DCLK1.2long	351-740	60.2 ± 0.1	16.5

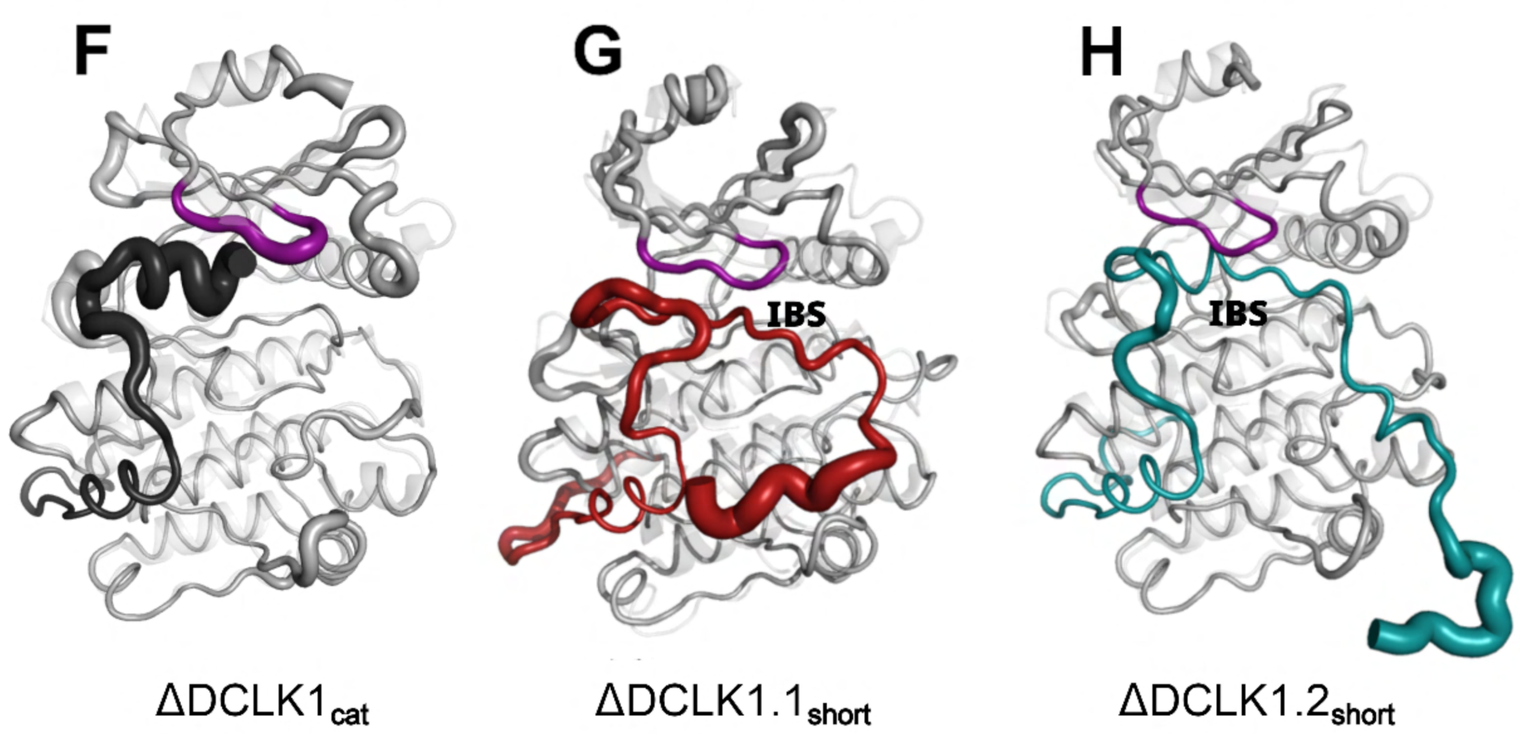

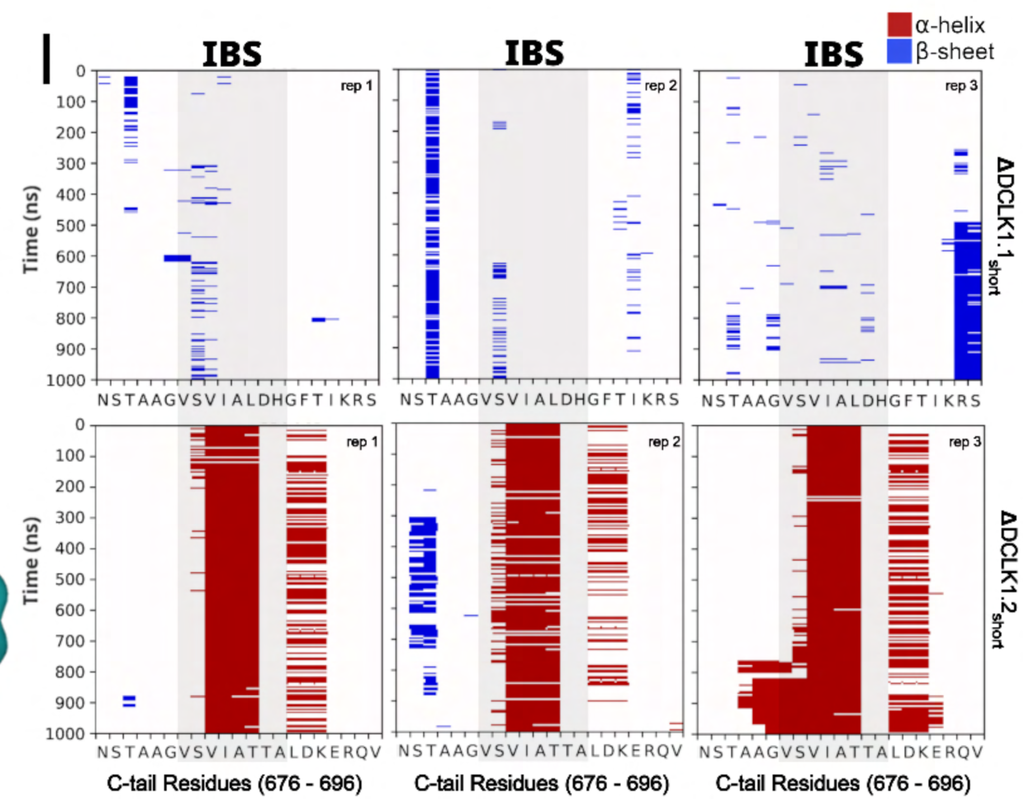

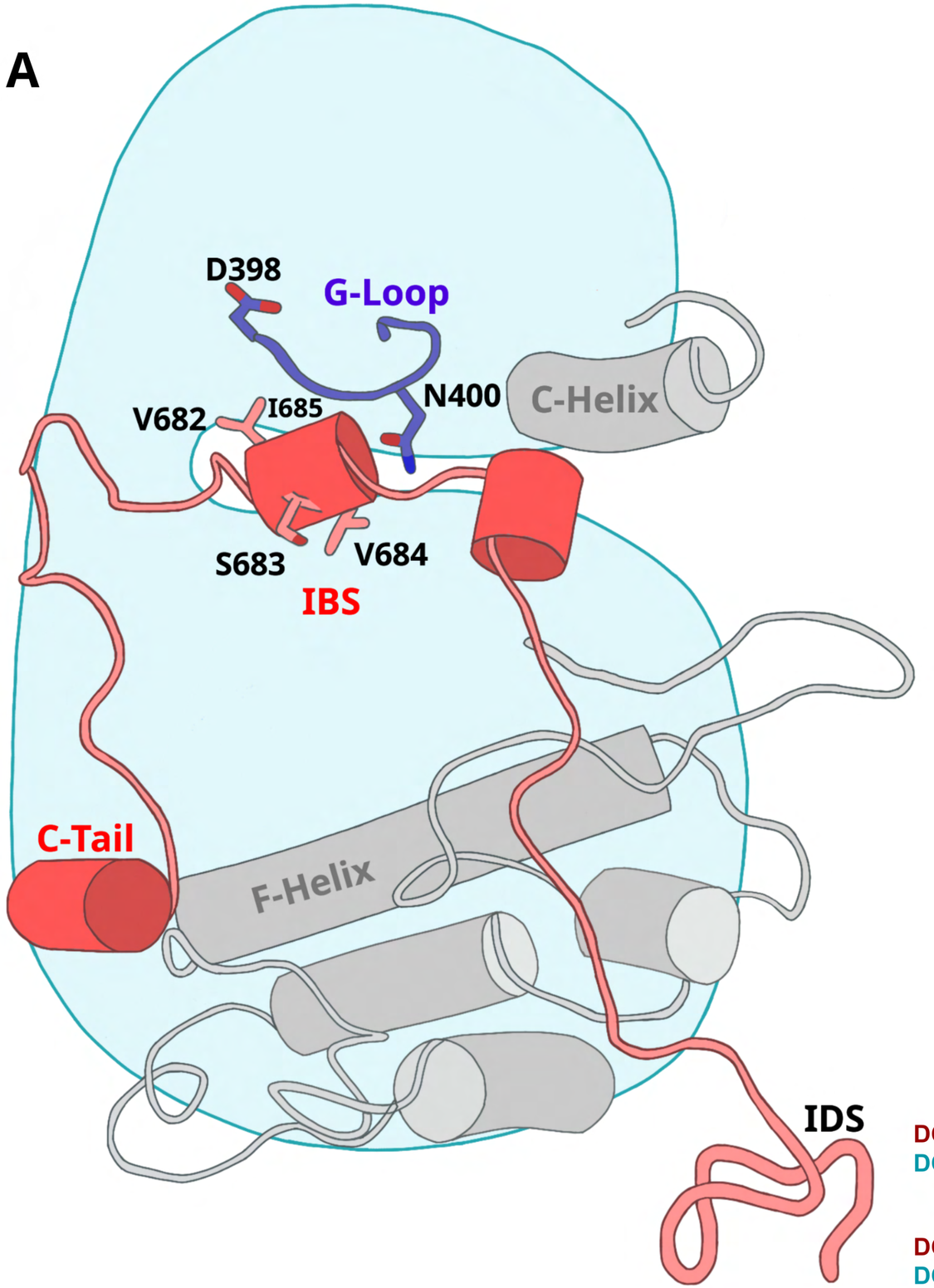
A
D398
G-Loop
N400
C-Helix
V682
I685
S683
V684
IBS
C-Tail
F-Helix
IDS

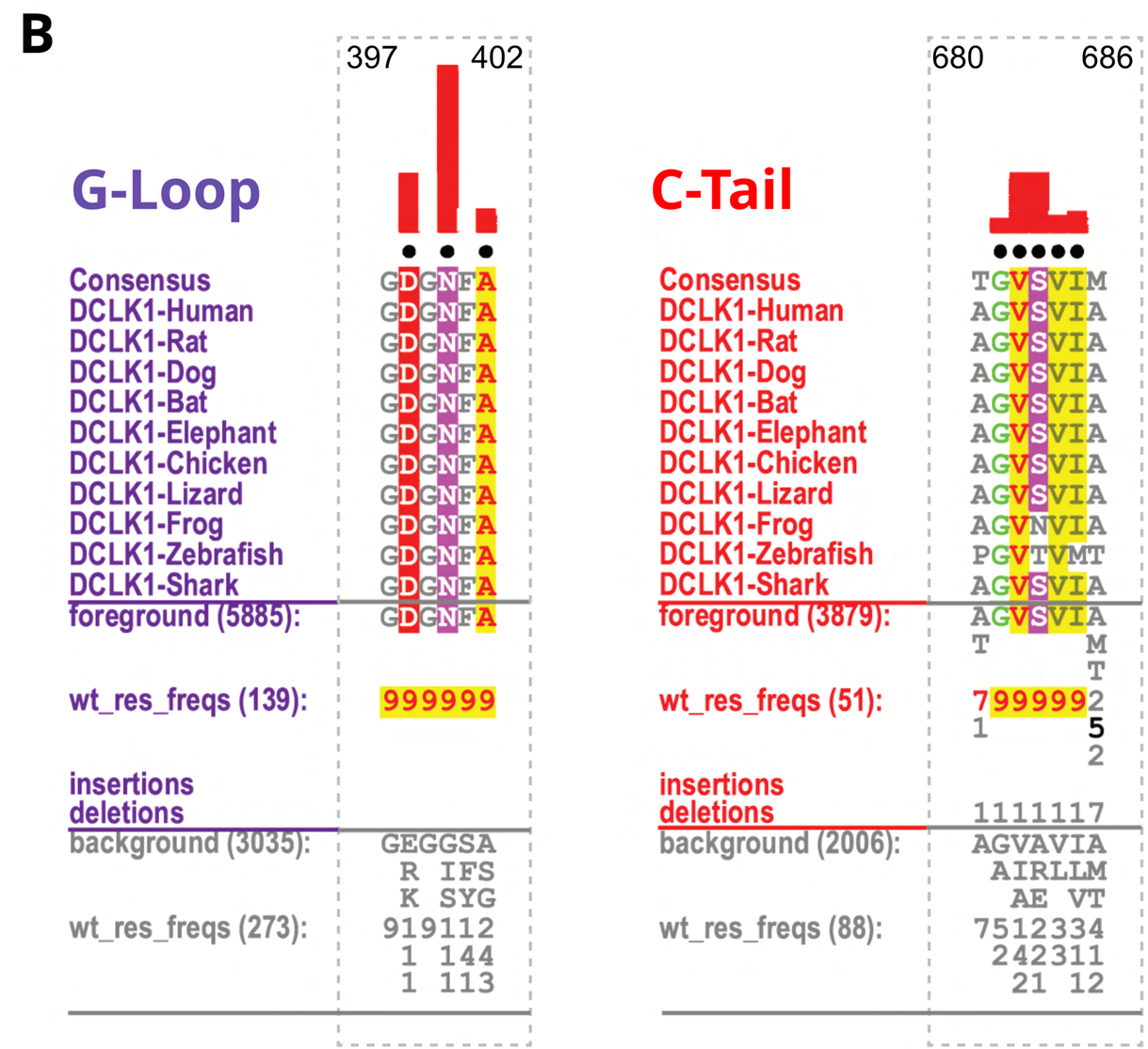
B
397
402
G-Loop
Consensus GDGNFA
DCLK1-Human GDGNFA
DCLK1-Rat GDGNFA
DCLK1-Dog GDGNFA
DCLK1-Bat GDGNFA
DCLK1-Elephant GDGNFA
DCLK1-Chicken GDGNFA
DCLK1-Lizard GDGNFA
DCLK1-Frog GDGNFA
DCLK1-Zebrafish GDGNFA
DCLK1-Shark GDGNFA
foreground (5885): GDGNFA
wt_res_freqs (139): 999999
insertions
deletions
background (3035): GEGGSA
R IFS
K SYG
wt_res_freqs (273): 919112
1 144
1 113
680
686
C-Tail
Consensus TGVSVIM
DCLK1-Human AGVSVIA
DCLK1-Rat AGVSVIA
DCLK1-Dog AGVSVIA
DCLK1-Bat AGVSVIA
DCLK1-Elephant AGVSVIA
DCLK1-Chicken AGVSVIA
DCLK1-Lizard AGVSVIA
DCLK1-Frog AGVNVIA
DCLK1-Zebrafish PGVTVMT
DCLK1-Shark AGVSVIA
foreground (3879): AGVSVIA
T M
T
wt_res_freqs (51): 799999 2
1 5
2
insertions
deletions 1111117
background (2006): AGVAVIA
AIRLLM
AE VT
wt_res_freqs (88): 7512334
242311
21 12

C
648
P
696
DCLK1.1 NDDGLPENEHQLSVAGKIKKHFNTGPKPNSTAAGVSVIA...LDHGFTI
DCLK1.2 NDDGLPENEHQLSVAGKIKKHFNTGPKPNSTAAGVSVIATTALDKERQV
697
740
DCLK1.1 .KRSGSLD....YYQQPGMYWIRPPLLIRRGRF...SDEDATRM.....
DCLK1.2 FRRRRNQDVRSRYKAQPA.....PPELNSESEDYSPSSSETVRSPNSPF

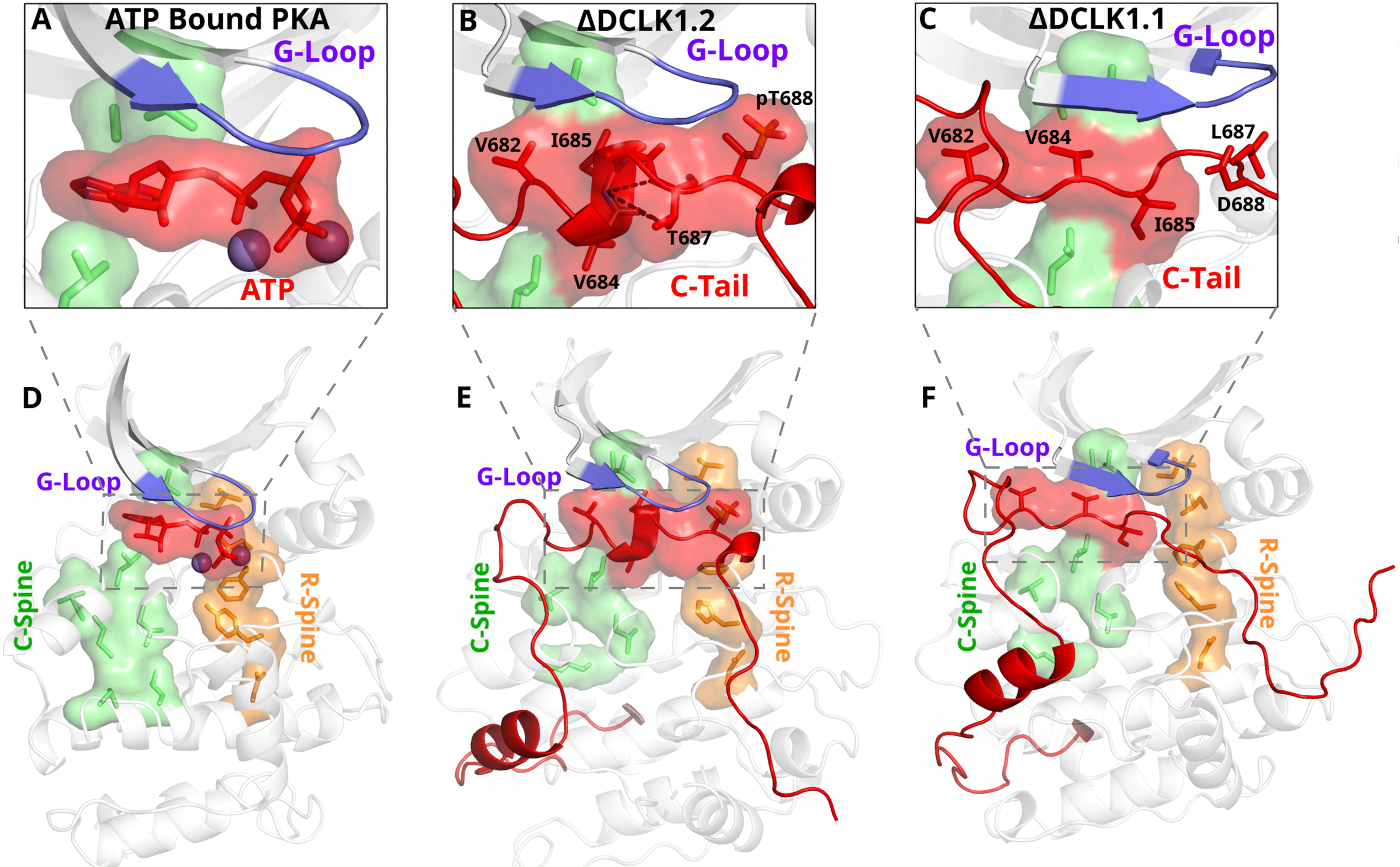

ATP Bound PKA
(PDB: 1ATP)

ΔDCLK1.2
(PDB: 6KYQ)

ΔDCLK1.1
(AlphaFold Model)

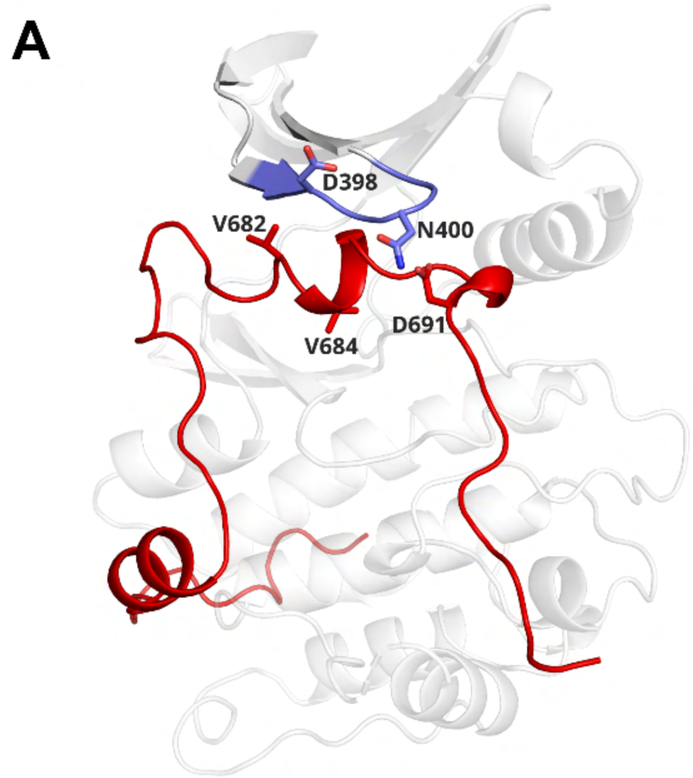

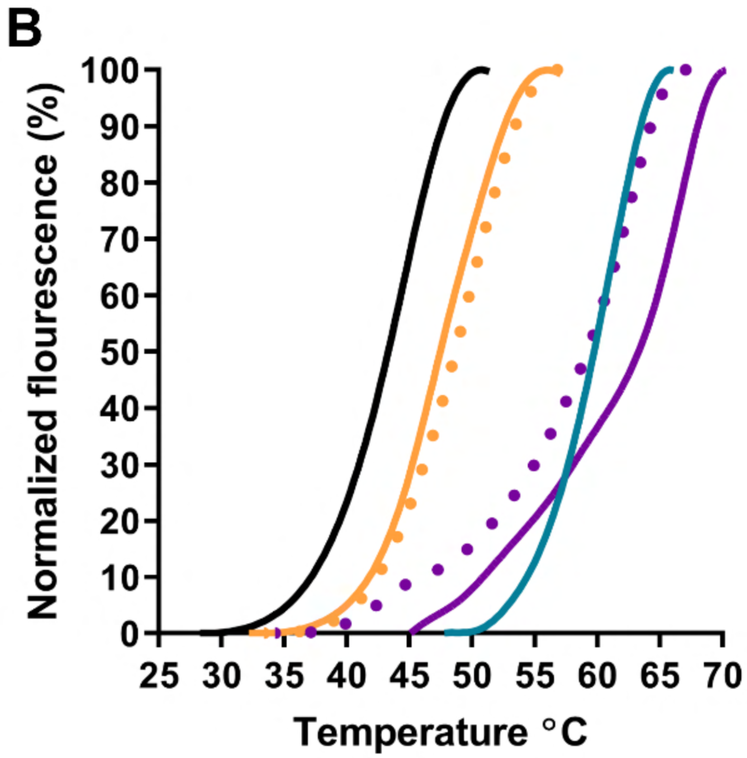

C

	Tm (°C)	ΔTm (°C)
DCLK1$_{cat}$	43.7 ± 0.1	–
DCLK1.2$_{351\text{-}703}$	60.2 ± 0.1	16.5
DCLK1.2$_{D398A}$	66.7 ± 0.1	23.0
DCLK1.2$_{N400A}$	63.6 ± 0.3	19.9
DCLK1.2$_{V682/684T}$	49.0 ± 0.1	5.3
DCLK1.2$_{D691A}$	47.8 ± 0.2	4.1

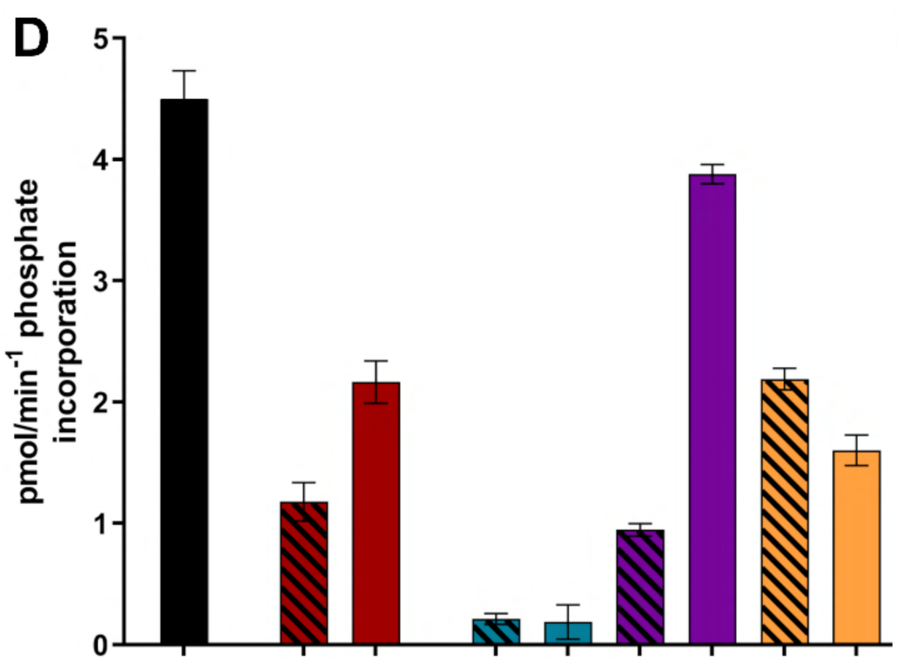

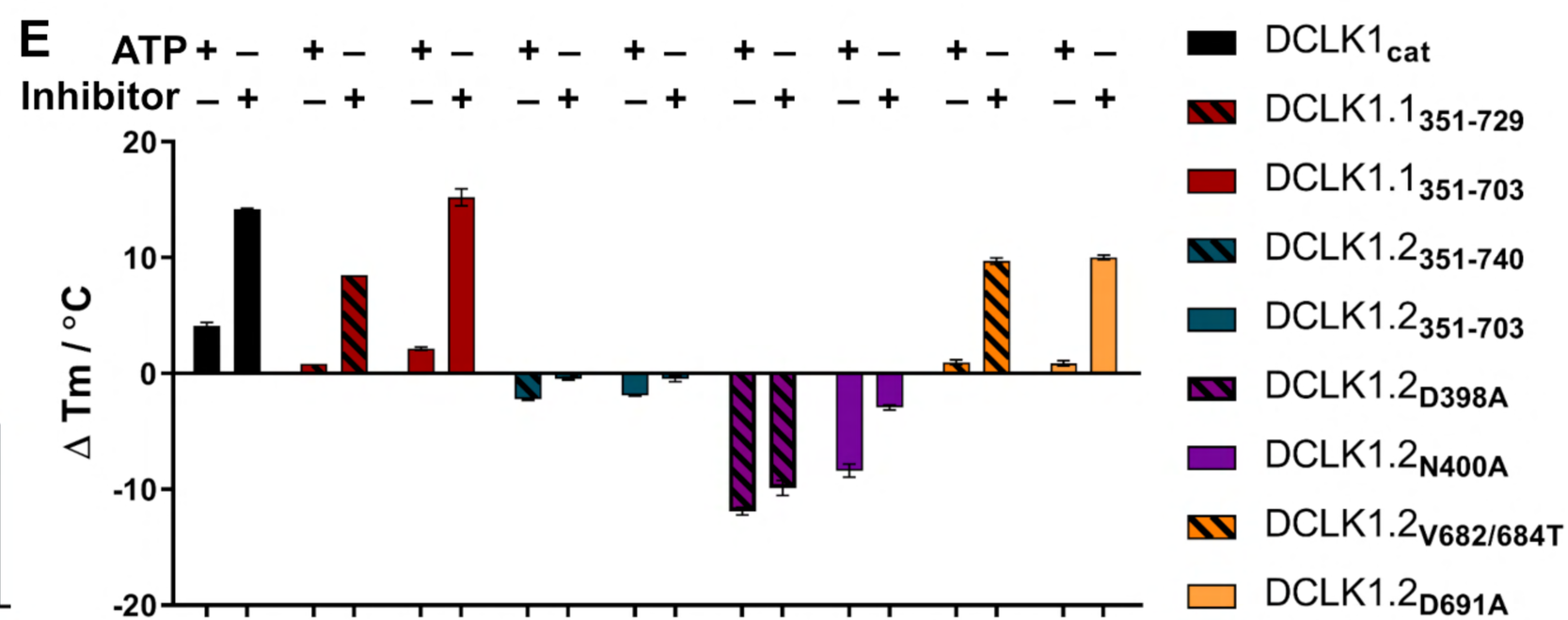

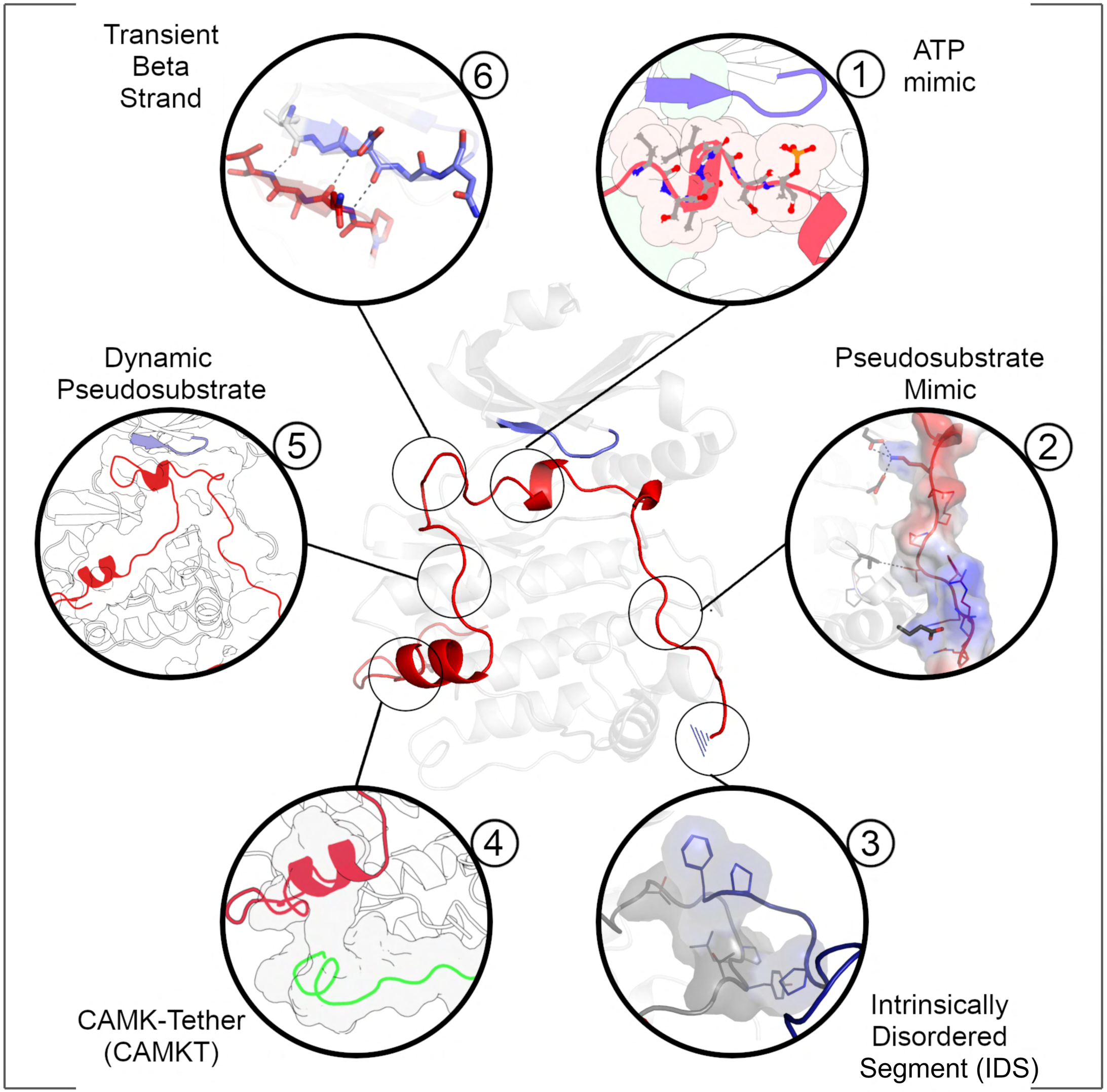
Shared between DCLK1.1 and DCLK1.2
Different between DCLK1.1 and DCLK1.2
Transient Beta Strand
6
ATP mimic
1
Dynamic Pseudosubstrate
5
Pseudosubstrate Mimic
2
4
3
CAMK-Tether (CAMKT)
Intrinsically Disordered Segment (IDS)